dynardo
dynamic software & engineering

ISSUE 2/2018

Title Story // Field-Metamodeling for Transient Electro-Thermal-Mechanical Applications

Simulations for Vertical Filling

Fatigue Life Analysis of an Exhaust Manifold

Cost and Function Optimization of a Proportional Solenoid

Design Optimization of Suspension Coil Springs

RDO-JOURNAL

optiSLang

SoS

esocaet

Upgrade your work, upgrade your life.

The career-integrated study programs enable engineers with bachelor's and master's degrees to obtain scientifically based and practice-oriented simulation knowledge.

Applied Computational Mechanics

Responsible Universities
- HAW Landshut and Technische Hochschule Ingolstadt, Germany
- PES University, India

Advancement Opportunities
- Master of Engineering (M.Eng.)
- Qualification in selected modules

Module Offer (excerpt)
- Nonlinear and Contact Analysis
- Materials and Material Models
- Computational Dynamics
- Fatigue and Fracture Mechanics
- Modeling Techniques
- Optimization and Robust Design

Computational Fluid Dynamics

Responsible University
- HSR Hochschule für Technik Rapperswil, Switzerland

Advancement Opportunities
- Certificate of Advanced Studies
- Qualification in selected modules

Module Offer
- CFD in Practice
- Fluid Dynamics and Heat Transfer
- Mathematics and Computational Methods

Computational Medical Engineering

Responsible University
- Witten/Herdecke University, Germany

Advancement Opportunities
- Certificate of Advanced Studies
- Qualification in selected modules

Module Offer
- Medical Fundamentals for Engineers
- Regulatory Affairs for Development of Medical Devices
- Biomechanical Simulation

Start your next career level now
www.esocaet.com/en/studies • +49 (0) 8092 7005-52

by CADFEM

FIELD-METAMODELING FOR TRANSIENT ELECTRO-THERMAL-MECHANICAL APPLICATIONS

In their lifetime, a lot of products are permanently exposed to environmental influences like changing climate, vibration or mechanically and thermally induced stresses. In addition, there are manufacturing tolerances, material scatter or other stochastic effects, which cause single scattering or spatially scattering properties of components and structures. To ensure product reliability and lifetime, to avoid product recalls and to meet safety requirements, these variations have to be taken into account in virtual prototyping by applying suitable statistical models and methods.

Because of the high computational effort, it is still a great challenge in simulation to consider all effecting influences. Consequently, for example, classic FEM methods often only use temperature-based lifetime models in virtual product development. Reduced Order Models (ROMs) and Field-Metamodeling can be applied in order to replace the immense simulation effort on the FE level. Thus, coupled thermo-mechanical simulations become applicable for further design optimization

The classical "physics-based" approach of ROMs uses a matrix condensation. However, this type of reduction is often only suitable for linear systems. A data-based ROM is also applicable for simulating complex nonlinear systems. The method uses function models for approximating the response variation based on the influence of all effecting input variations and depending on a pre-investigated window of input parameter variation. Here, Field-Metamodels (F-MOP) can be used to approximate signals, FEM solution field variables or geometric deviation fields.

Statistics on Structures combined with optiSLang provides automated solutions for the generation, validation and visualization of F-MOPs. The prediction measure Field-Coefficient of Prognosis (F-CoP) indicates at which location the F-MOP has a high or low prediction quality. This knowledge can also be used to quantify the influence of scattering field inputs on scattering field responses.

The title story of this RDO-Journal illustrates a coupled transient electro-thermal-mechanical fatigue analysis of aluminium bond contacts enabled by metamodeling technology. By using Field-Metamodels, a high approximation quality could be achieved and real life load signals could be evaluated in almost real-time. Thus, not only lifetime was verified, but also the integration of lifetime tracking into digital twins becomes possible.

Apart from that, we again have selected case studies and customer stories concerning CAE-based Robust Design Optimization (RDO) applied in different industries.

I hope you will enjoy reading our magazine.

Yours sincerely

Johannes Will
Managing Director DYNARDO GmbH

Weimar, October 2018

CONTENT

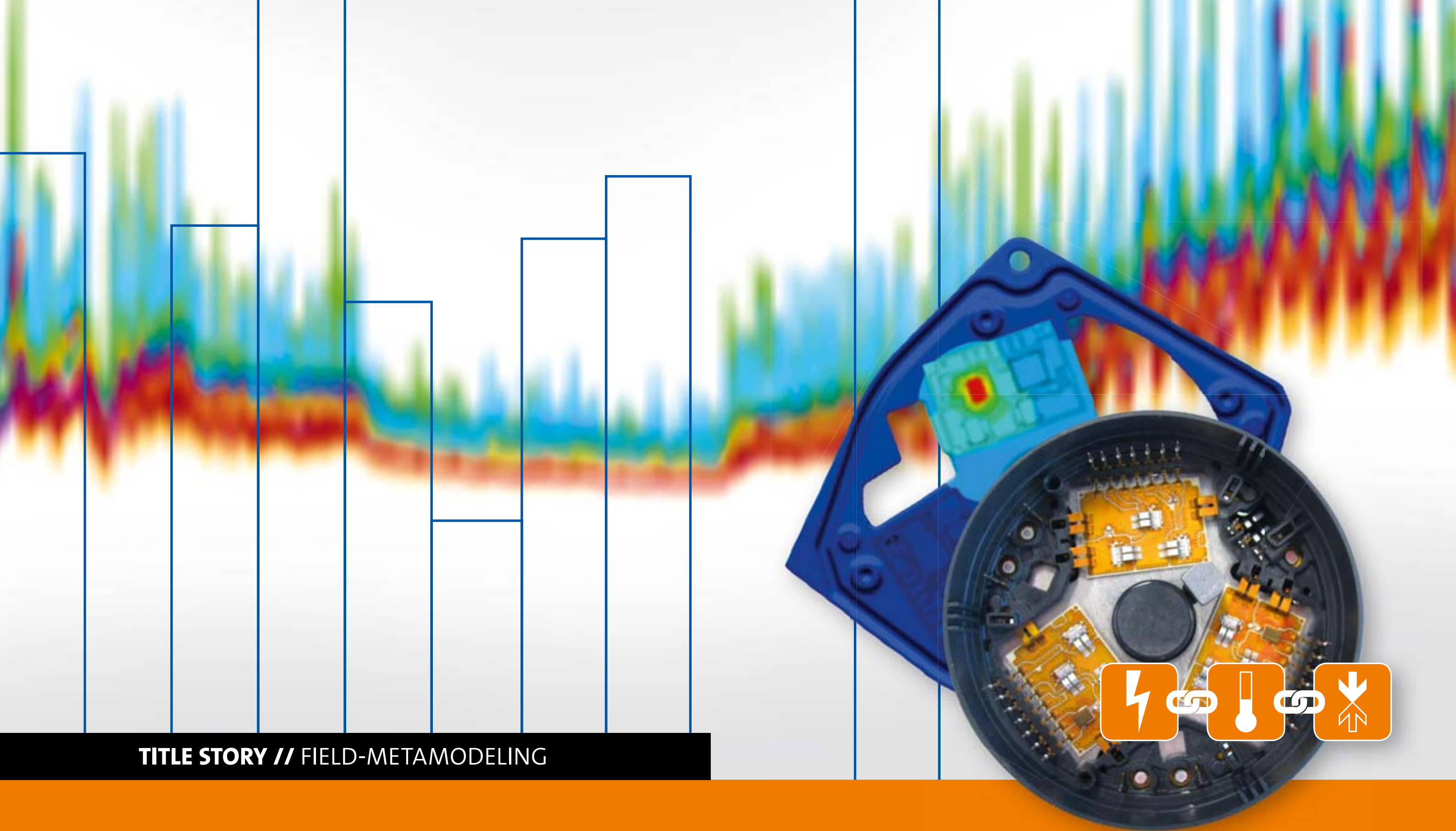

FIELD-METAMODELING FOR TRANSIENT ELECTRO-THERMAL-MECHANICAL APPLICATIONS

At Robert Bosch GmbH, metamodeling was applied as an alternative to electro-thermal-mechanical FEM simulation in order to accelerate the assessment of temperature fields or contact stresses.

Introduction

Electronic circuit boards are used in a wide variety of engineering applications. In the automotive industry, for instance, they can be found in electronic power steering assemblies. This case of application was also used as a test vehicle for the method that is described in this article. Other examples are battery load control circuits, motor control or safety devices like traction control and ESC. These circuit boards are constantly exposed to environmental influences like changing climate conditions (humidity), hazardous chemical conditions, vibration and mechanically and thermally induced stresses.

The goal in predictive engineering is to assess mechanical designs with respect to real world load cases. It should be possible to create and validate engineering designs with a verification of operational readiness during the full product lifetime.

One area of interest in that regard is the fatigue analysis of aluminium bond contacts during load cycle operations. Here, transient input signals originating from the bus system, e.g. steering or brake controls, as well as changing environmental conditions, lead to mechanically and thermally induced strain. Due to deviating stiffnesses and thermal coefficients of expansion at the electrical contact area (see Fig. 1), the aluminium bond contacts might fail, which is not acceptable in safety-critical applications.

State of the art in computer aided design is the fully coupled FEM analysis using design platforms, such as ANSYS Workbench, to model the thermo-mechanically coupled electric circuit board under different loading conditions. For the broad range of real-world load cases, it needs to be considered that, during the design phase, fully coupled transient simulations have been infeasible yet. Using the FEM method, only temperature-based lifetime models are applied in industrial applications, due to the large computational demand. The next evolution is a design assessment based on a full thermo-mechanical coupling (see Fig. 2), but in order to use this approach effectively, much more efficient solution techniques need to be developed.

This article demonstrates how a fully coupled transient electro-thermal-mechanical FEM simulation can be replaced by metamodeling technology. First, the field solution quantities are expressed using shape decomposition techniques. Based on a design of experiment, the resulting shapes of the design space are then used to generate a field-metamodel that

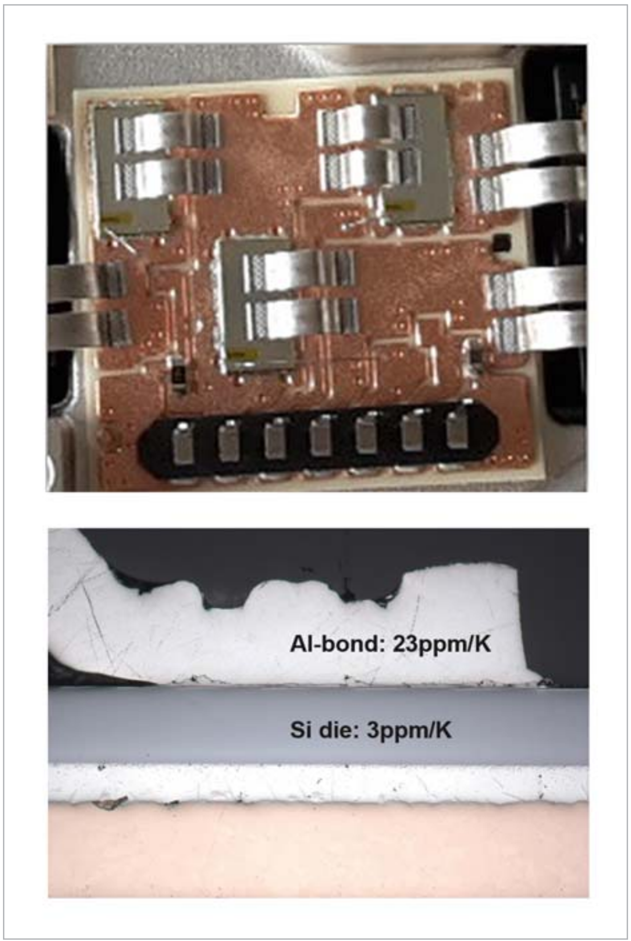

Fig. 1: Circuit Board with electric aluminium bond connections

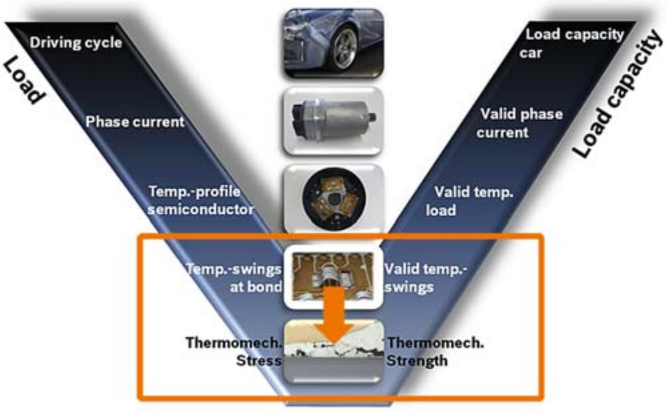

Fig. 2: Next step in lifetime modeling from temperature-based to thermo-mechanical models

can be applied to very rapidly compute new transient field responses, like temperature fields or normal contact stresses. The results are then implemented into a rain-flow counting routine to make design decisions based on the complete transient field response in almost real-time (see Fig. 3).

Methodology

Field-Metamodeling

Scalar based metamodels are used in engineering as handy surrogate models. Due to their good mathematical foundation and ease of application, they are widely accepted in the engineering community. These surrogate models are not only applied as a replacement for the complex and error prone large-scale simulation models, but also for gaining a general knowledge of the non-linear correlation of the corresponding input and output parameters. Metamodels can be used to gain engineering knowledge and often give the design engineer the key insight into what really influences the design response.

Field-metamodels are a natural multi-dimensional expansion to the idea of scalar based metamodels. Instead of the simpler one-dimensional scalar input-output response correlation modeling (e.g. nodal stress at a time instant, scalar integral quantity, maximum deflection, as well as

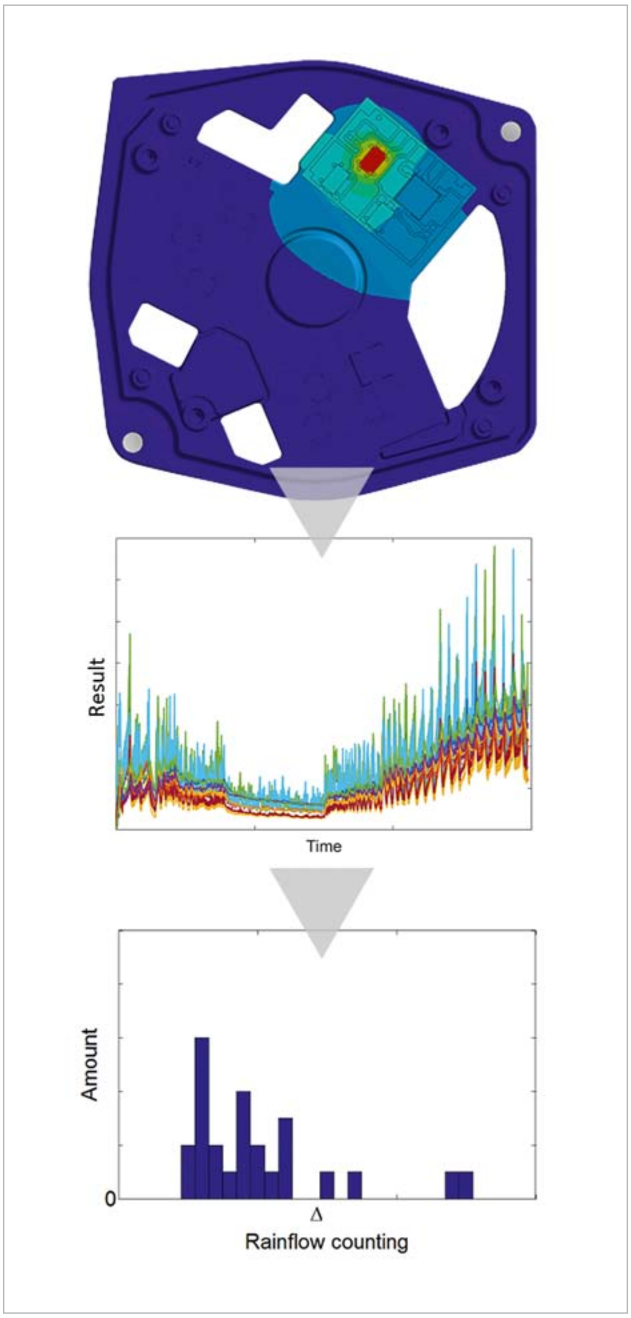

Fig. 3: Rainflow counting for field result quantity

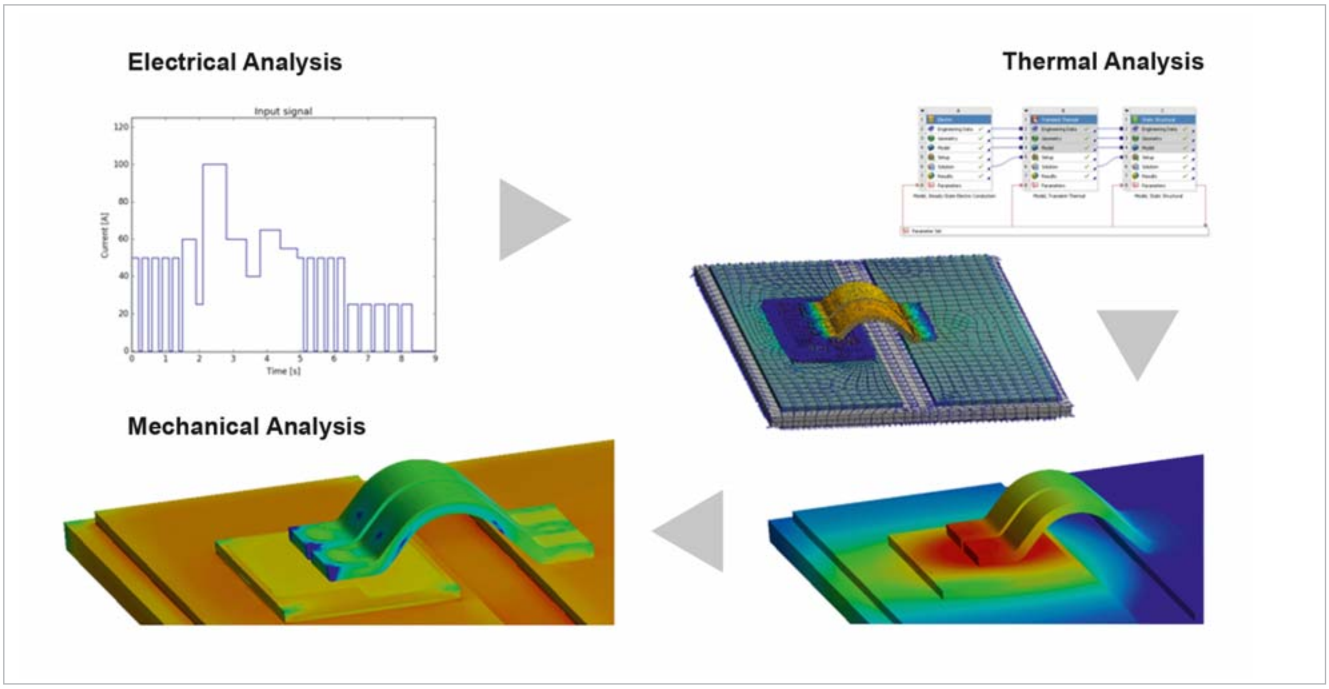

Fig. 4: Coupled transient Electrical-Thermal-Mechanical ANSYS Workbench model

stress for a complete domain) the field-metamodel generates a surrogate model for the full field response. The method is based on a Karhunen–Loève like decomposition of the field quantity in the parametric design space, which is later daisy-chained by using non-linear models.

In the current example, the full temperature and stress fields are expressed with this type of model. As an advantage of this approach, the design engineer does not need to pin-point one specific location of interest, before he builds the surrogate model. Furthermore, changing locations of interest during a transient analysis, e.g. hot spot analysis, becomes much more feasible.

Sensitivity Analysis

Fig. 4 demonstrates the underlying FEM simulation workflow generated in ANSYS Workbench. An electrical input signal is applied in an electric field simulation. The eddy currents act as source terms for the transient temperature computation. This data is subsequently fed into a thermo-mechanical stress strain simulation.

The resulting field-metamodel is based on a parametric scan of the underlying design space. It is important to note that electric loading leads to different temperature fields, depending on the load history. Therefore, a transient parametrization has to be generated to capture these effects. The input space consists of environmental conditions, e.g. ambient temperature and the electric loading signal, for which an appropriate partitioning scheme was devised. Afterwards, an Advanced-Latin-Hypercube sampling is used to generate a design of experiments that captures the underlying design space of the fluctuating current input signal. The parametric agglomeration of input to field-output data finally builds the foundation of the field-metamodel.

Transient field surrogate model

The basis of the field surrogate model is a shape decomposition of the quantity of interest. Fig. 5 visualizes the first three expansions of the normal stress field of the aluminium bond contact surface. Any response field of the underlying design space might be decomposed into such prototype shapes. Together with the information of the input parametrization of the design of experiments, a surrogate model can now be built. The resulting metamodel can now be used to generate field responses for new input sets and to

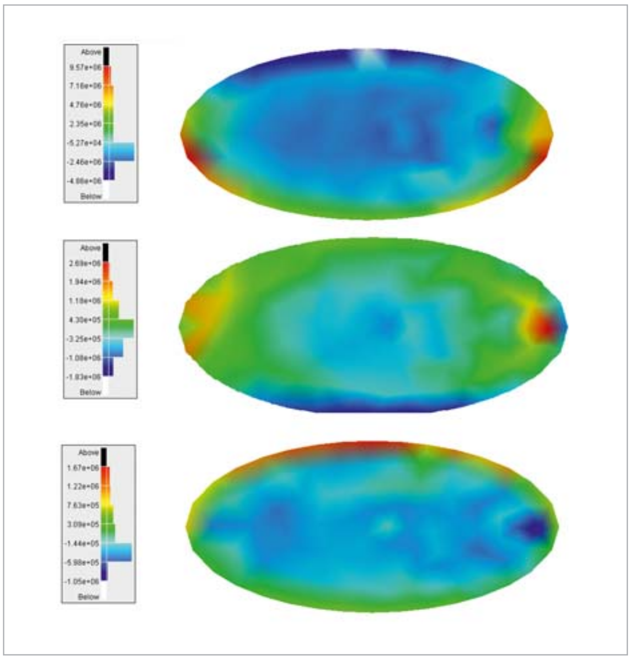

Fig. 5: First three shapes of metamodel stress field decomposition in normal direction for the bond contact surface

visualize the non-linear input-output correlation, much like their scalar companions. Additionally, a multi-dimensional Coefficient of Prognosis (CoP) value is available for the domain, which demonstrates the model approximation quality at each location of the model (see Fig. 6).

The input parametrization of the design of experiments results in a scalar input to multi-dimensional field output mapping. In the beginning, it was stated that the history of the applied loading affects the outcome of the experiment. Put differently, the current input signal and the temperature

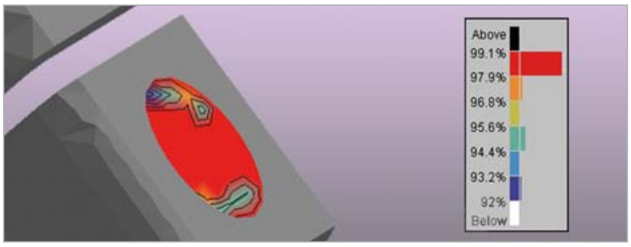

Fig. 6: Field-CoP values for metamodel of stress field in normal direction for the bond contact surface

field at each position affect the next temperature approximation. Therefore, the temperature is not only considered as an output, but also as an input. The above-mentioned decomposition technique is therefore applied to the temperature state at each beginning of a parametrized load step to generate a unique field decomposition. The enlarged design space is then used to generate a field-metamodel, which is not only based on the scalar input quantities, but it also relies on the temperature field information on the full domain at the beginning of each load step.

optiSLang custom input integration

The resulting field-metamodel can be used inside of standard optiSLang workflows. A custom input integration was developed (see Fig. 7) to allow users to enter text-based load cycle data and generate a full field response, which is based on the transient approximation as defined above. The choice of custom integration interface also allows non-experts to use these surrogate models. Thus, they can make engineering decisions without having expert simulation knowledge. Results can then directly be stored using simulation data management technology to ensure traceability and to make them available to other stakeholders like circuit board designer and project management.

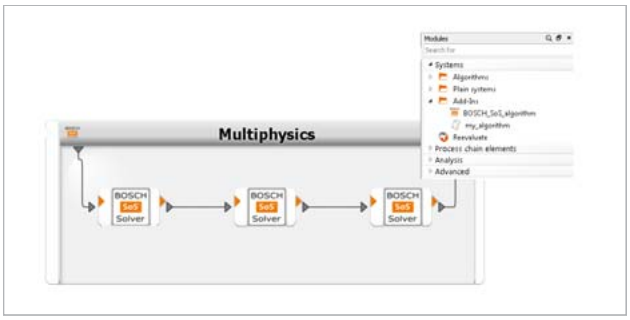

Fig. 7: Use of custom algorithm integration node in optiSLang for an easy use in user defined workflows

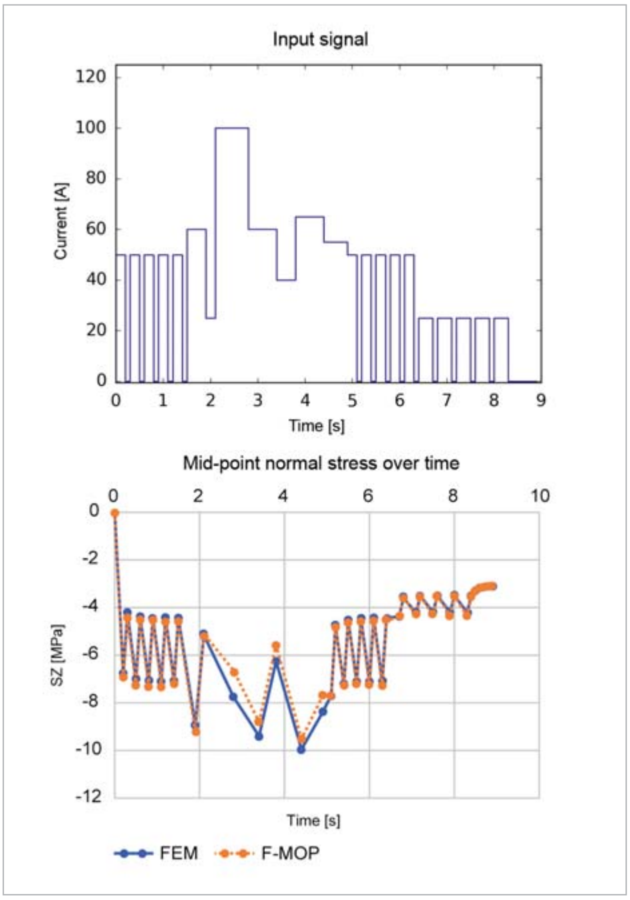

Fig. 8: Comparison of transient stress field solution at bond contact surface using FMOP-surrogate model to full FEM model

Results and discussion

The field-metamodel technology has been effectively applied in the design of electric circuit boards. Fig. 8 shows how the normal stress on the inside of the bond contact surface changes as a function of a varying input current load signal. The output of the transient surrogate model (dashed line) matches very closely the response of a fully coupled FEM simulation (continuous line). For this specific example, the computation time could be reduced from around 25 hours for the FEM model to approximately two minutes using the field-metamodel. For longer profiles, FEM will no longer be feasible and the benefit of the metamodel will be even bigger.

The surrogate model can be used to fully replace a complex FEM simulation, while significantly reducing the computational demand. With this approach, thermo-mechanical analysis as the next step in lifetime-based modeling becomes reality. It furthermore demonstrates that real-time or almost real-time digital twin applications are practical and feasible.

Authors //
K. Riester (Robert Bosch GmbH), S. Klonk (Dynardo GmbH)

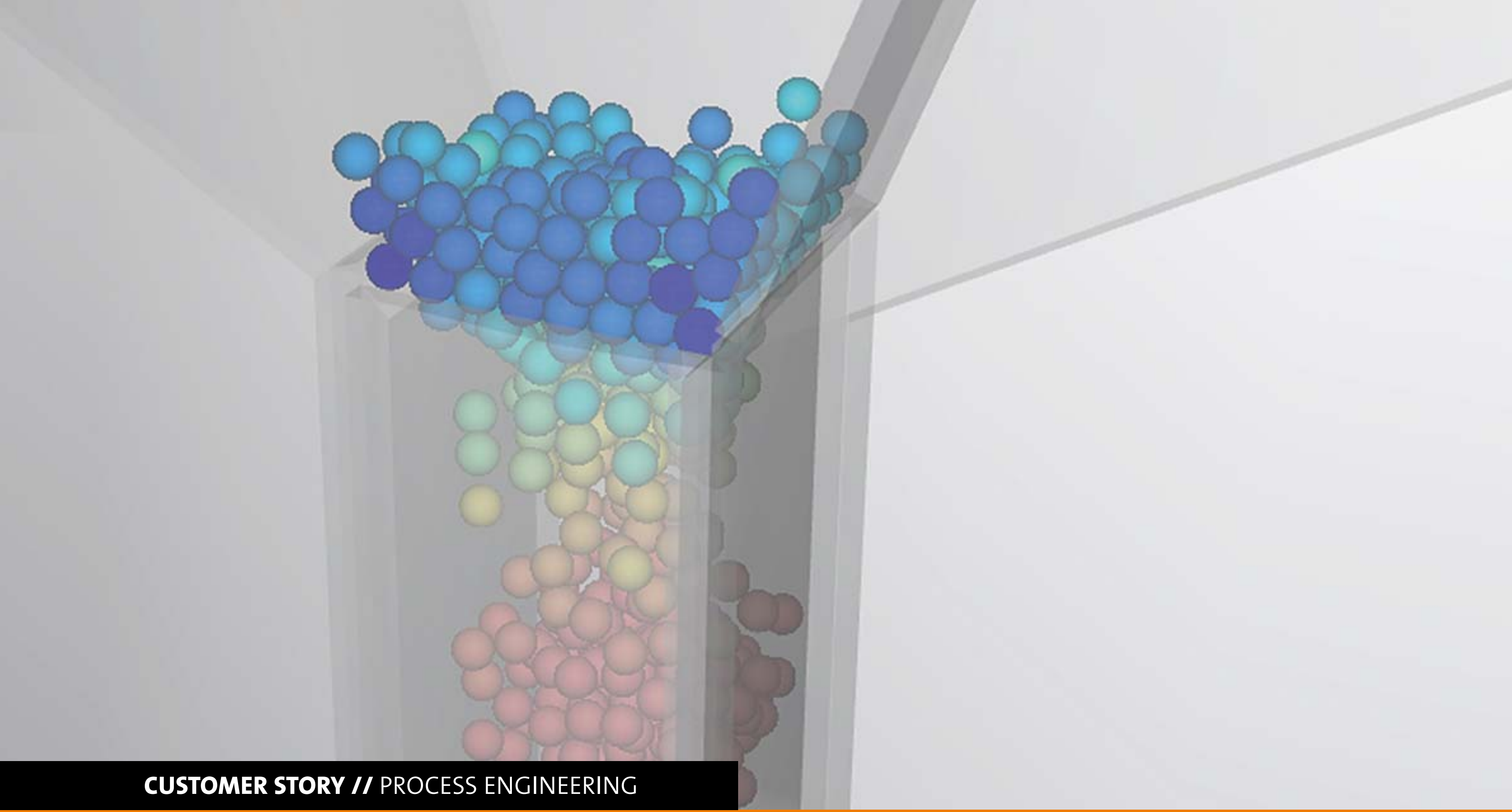

CUSTOMER STORY // PROCESS ENGINEERING

CALIBRATION OF DEM SIMULATIONS FOR VERTICAL FILLING: HOW TO HANDLE RANDOMNESS

At Robert Bosch Packaging Technology, optiSLang was used in conjunction with Rocky DEM to obtain accurate models for the simulation of vertical filling of granular foods.

Introduction

Vertical filling

Vertical filling is a flexible process and commonly used in industrial packaging of granular foods, such as candy, snacks and bakery goods. The process is shown schematically in Fig. 1. By increasing the frequency of drops of granulate portions, the output rate can be easily increased. However, the time distance between the portions must be kept large enough so that there is enough time to perform sealing. Otherwise, particles get caught between the sealing jaws, which often results in need for maintenance. Thus, compact falling of the portions is important for keeping the process reliable.

Discrete Element Method (DEM)

1. Overview

The Discrete Element Method (DEM) simplifies contacts by assuming particles to be stiff. Deformation is implemented by allowing a small overlap between particles. Contact forces are then calculated with simple relations to the current overlap. A variety of contact models is available in different DEM implementations. The model used here is the linear hysteresis model developed by Walton and Braun [1, 2] (Fig. 2).

2. Model Calibration

Identifying model parameters for DEM simulations is challenging [4, 5]. An attractive and commonly used method is numerical model calibration, which consists of varying the model parameters while comparing the simulations to experimental results until reality is reproduced to a satisfactory extend. Calibration is usually performed in a relatively simple representative experiment [6]. A consecutive validation step can be then performed to verify if the model parameters hold up in the actual process of interest.

3. Solver Noise

Since granular systems are highly chaotic, small variations in initial conditions, such as the precise positions of individual particles in the collection bin before the drop [3], can dramatically affect the process outcome [7]. Physical randomness, just as process design, can be of great importance in achieving a desirable outcome and avoiding unfavorable ones. This is true for the physical process as well as for the simulations.

Goal

For this study, model parameters for a granular sample food had to be found. The chosen good was sugar-coated, bite-

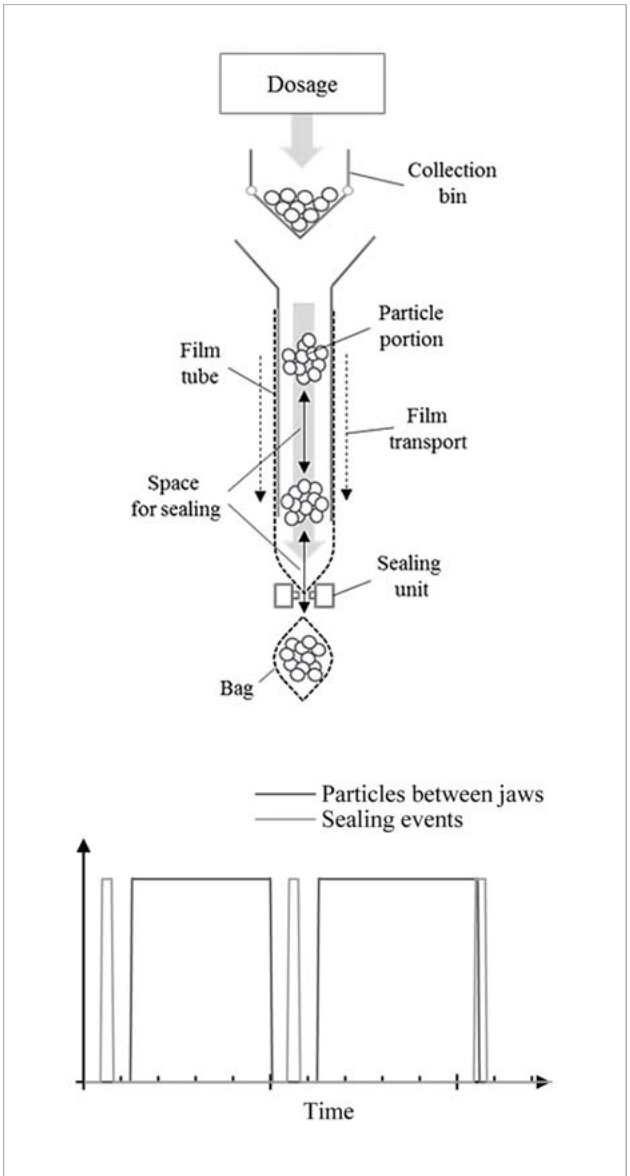

Fig. 1: The vertical filling process. Schematic overview over process principle. Successful sealing (bottom left) and likely defect due to particles getting caught in the sealing unit (bottom right)

size chocolate candy with a porous cookie core. As calibration trial, a drop test that is very similar to the industrial process was used representing in-situ calibration [5]. Further, the necessity to incorporate the physical randomness in the DEM simulations and their effect on the calibration was evaluated. Finally, the methods were compared with regard to their feasibility, robustness and accuracy.

Experiment

The drop setup has been described in [3] and is shown in Fig. 3. Two rectangular falling tubes with different inner areas A□,1 and A□,2 where available. By varying the sample mass, a total of three scenarios were performed (Table 1).

The experiment was initiated by opening the flaps at the bottom of the sample container. The time stamps of the first and last particle leaving the tube at the bottom were

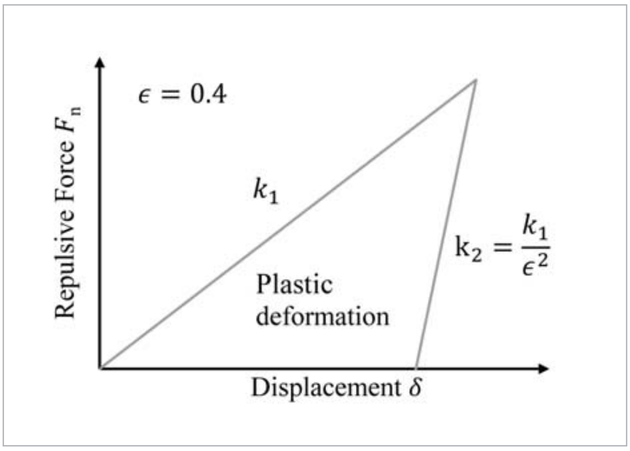

Fig. 2: Relationship between particle δ overlap and Force F_n for restitution coefficient ε=0.4 (from [3])

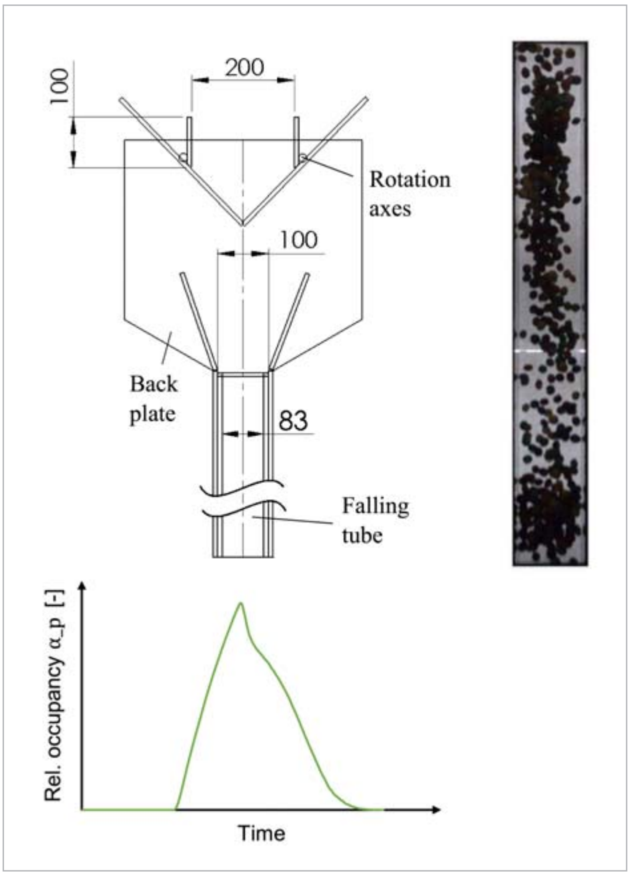

Fig. 3: Drop setup described in [3] and snapshot of drop test. Measures in mm

Sample mass	Inner tube area	Used for
500g	A□,1=76 cm²	Calibration
	A□,2=100 cm²	Validation
700g	A□,1=76 cm²	Validation

Table 1: Scenarios of the drop test

recorded. The difference between these residence times Δt_{res} is equivalent to the portion range τ_{rg} discussed in [3].

$$\tau_{rg} = \Delta t_{res} = t_{res,lp} - t_{res,fp}$$

Then, the degree of filling α_p of the tube was tracked over time and normalized to the maximal possible value (entire tube filled). Fig. 3 (see previous page) shows a frame cropped to the tube and the relative particle occupancy α_p plotted over time.

Simulation

Discrete Element Method

The experimental design (see chapter Experiment) was replicated with CAD tools and imported into the DEM environment. The pieces of candy were nearly spherical, so a spherical particle representation was chosen. The average sieve diameter of the particles was used as the sphere's diameter.

Young's modulus was chosen with regard to numerical criteria (computational cost and numerical stability) and left constant at 10^8 Pa [8]. The calibration parameters x (Table 2) were friction coefficients μ, respectively for the static (sticking) and the dynamic (sliding) case and the coefficients of restitution ϵ. Each parameter was assumed different for the interaction between the particles (P-P) and the interaction between particles and the boundary (P-B). Additionally, a factor for rolling resistance was calibrated to account for the increased rolling of spherical particles compared to the real particles [9]. The eventual model parameters x differ from the "true" physical parameters due to model shortcomings [10, 11].

Parameter	Material and Scenario		Symbol
Friction	Particles – Particles	Static	$x_1 = \mu_{s,P-P}$
		Dynamic	$x_2 = \mu_{d,P-P}$
	Boundary – Particles	Static	$x_3 = \mu_{s,P-B}$
		Dynamic	$x_4 = \mu_{d,P-B}$
Restitution	Particles – Particles		$x_5 = \epsilon_{P-P}$
	Boundary – Particles		$x_6 = \epsilon_{P-B}$
Rolling Resistance	Particles		$x_7 = RR$

Table 2: Calibration parameters

Calibration

The goal of model calibration is to identify the parameter set x that produces the best match between simulations w and the experimental results u. For the drop test, we aim to accurately predict the portion range τ_{rg} from the experiment. This goal can be formulated as an optimization problem, where the error between the simulation and the experiment has to be minimized. Several optimization strategies have been used for DEM model calibration, such as manual comparison [12], gradient-based methods [13], genetic algorithms [14] and Artificial Neural Networks [4]. A recently followed approach is to create a metamodel with a kriging algorithm from several anchor points in the parameter space and perform the optimization on the resulting surrogate model [15].

The benefit of the latter method is that the number of solver runs can be reduced and evaluation of the goal function on the surrogate model is quick.

The procedure was implemented in an automated calibration workflow (Fig. 4) in optiSLang. The DEM solver was called at different parameter sets (samples) and the results were compared to the experimental data. The data was then processed into a metamodel of the solver behavior.

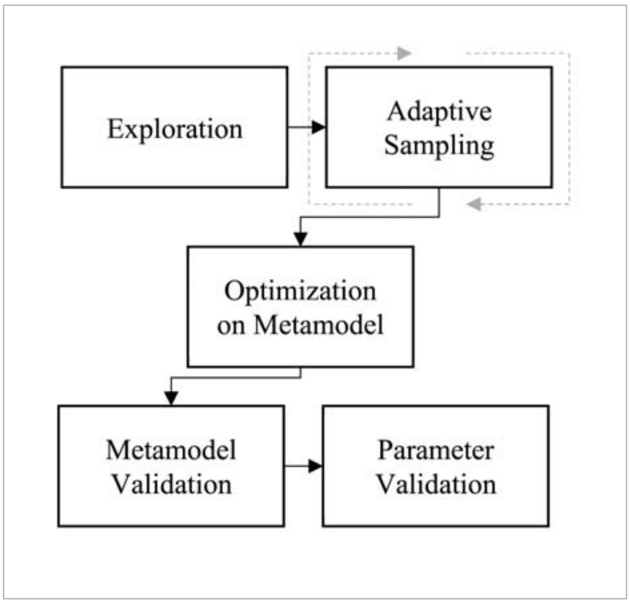

Fig. 4: Calibration Workflow in optiSLang

1. Metamodeling

Kleijnen [16] gives a comprehensive theoretical overview over metamodeling methods, so we will use part of his nomenclature here. The solver output w has to be approximated by the output $\widehat{w}$ of the metamodel f_{meta}.

$$w = f_{sim}(x,r) = f_{meta}(x) + e$$

f_{sim} is the noisy solver function which depends on the calibration parameters x and the seed of the random number generator r. The metamodel function is f_{meta} with its value depending only on the calibration parameters x. e is the residual vector, in which the local error of the metamodel at anchor point i is

$$e_i = \widehat{w} - w_i$$

If we make the assumption, that the kriging algorithm is capable of describing the behavior of a deterministic solver $f_{sim}(x)$, there must be an kriging parameter set β which provides optimal fidelity. However, we must keep in mind, that we only have a finite amount of anchor points n to work with, so we can only find an estimate $\hat{\beta}$ of β. [16]

In the case of a noisy solver $f_{sim}(z,r)$, the regression will smooth out some of the solver noise [17, 16], while producing greater residuals than in the deterministic case. This does not imply bad quality of the metamodel but rather highlights the deterministic nature of f_{meta}. The criteria after how many simulation run the metamodel should be finalized is not obvious here. A possible criterion is to track the mean residuals over the number of anchor points n and stop the process when stagnation is reached. It is however not guaranteed that this point will coincide with an acceptable quality of $\hat{\beta}$.

2. Adaptive Sampling

Choosing the anchor points with Latin Hypercube sampling (LHS) [18, 19] allows a sufficient coverage of the parameter space, while avoiding undesired sampling effects at a smaller number of anchor points [20]. However, DEM simulations are computationally expensive, so adaptive sampling, similar to [21], was performed to further reduce the number of solver calls.

The general topology (i.e. global trends) of the metamodel can be estimated quite well in an exploration phase with relatively coarse sampling. In a refinement iteration, we can add anchor points in the interesting regions of the metamodel (i.e. where the predicted error $\Delta\tau_{rg}$ between simulation w and experiment u is low) and recalculate the metamodel. With the refined information on promising zones, we can then repeat the refinement for several iterations until stagnation is reached or the maximum computation budget is spent.

3. Optimization

Kriging models are smooth. Therefore, fast gradient based approaches can be used for optimization [21, 22]. The implementation of the Lagrangian NLPQL solver of optiSLang was used due to its numerical performance and accuracy [23, 24].

Validation

There are two sources for errors in the calibration process: numerical (insufficient metamodel quality) or systematic measurement errors and shortcomings in the DEM model. To exclude both, two separate validation steps were performed.

1. Metamodel Validation

In order to ensure the prediction capability of the metamodel, a set of m validation simulation runs were performed at the supposed minimum x_{opt} and their results $w_1, w_2 ..., w_m$ were averaged. The difference $e_{opt} = \hat{w}_{opt} - \bar{w}_{opt}$ is a teller for the reliability of the metamodel at that point. If the error is unacceptably high, more anchor points should be added to increase the accuracy of $\hat{\beta}$.

2. Parameter Validation

To verify that the obtained parameter set x_{opt} was viable outside the calibration scenario, validation simulations were performed in the respective scenarios shown in Table 1 (see p. 7) The results were obtained from m averaged simulation runs.

3. Randomness

In real-life, the filling of the containers is a random process that cannot be reproduced in the next run, resulting in a partially random initial condition (RIC) of the bulk. This randomness is a physical property of the processes, influencing the outcome of the experiment.

The simulations were designed to account for that randomness, so a random and flat particle bed was created in the simulations before release. This added computational cost of around 37 seconds to the runtime of 110 seconds per run on average (34%). Furthermore, the RIC increases solver noise.

Both increased cost and solver noise are undesirable from an engineering standpoint, while it is unclear if the physical randomness actually plays a significant role and if the additional effort is justified. In order to determine whether the implementation of the physical randomness is actually necessary, we also performed the calibration with an arbitrary but constant initial state (CIC).

Results

Table 3 shows the number of anchor points (simulated parameter sets) over the iterations. Fig. 5 (see next page) shows a projection of a graphical representation of the metamodel after different iterations 1 and 10. The parameters found to be the most influential on the portion range τ_{rg} were $\mu_{d,P-B}$ and RR. All other parameters are held constant near their respective optimum for low DEM model error. We observe only a slight change in the topology of the metamodel between Iteration 1 and 10. This suggests that the sampling could be stopped after iteration 1.

However, to gain insight into the quality of the prediction of the metamodel, we also must assess the residuals e

	Iteration 1 (Exploration)	Itertion 3	Iteration 10	Iteration 20	Average per Iteration*
n_{rnd}	290	379	693	1162	46
cost	11.8 h	15.4 h	28.2 h	47.3 h	1.9 h
n_{cnst}	289	378	698	1143	45
cost	9.1 h	11.5 h	21.3 h	34.9 h	1.4 h

Table 3: Number of anchor points n and total computational cost of the calibration in the drop test at different iterations | *after iteration 1

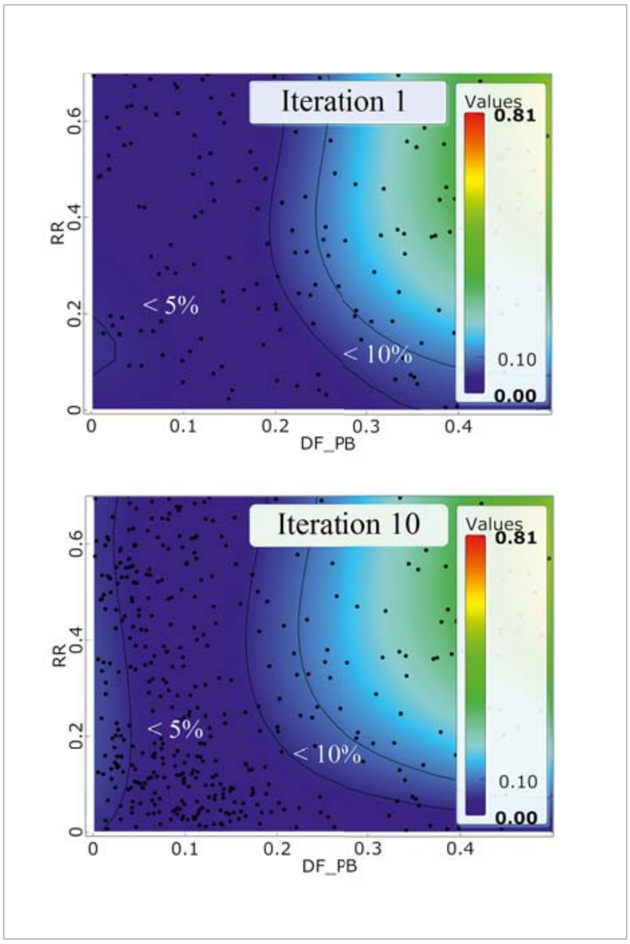

Fig. 5: 2-dimensional projection of the 7-dimensional metamodel for $\Delta\tau_{rg}$ in % in relation to the two most influential parameters (RR and $\mu_{d,P-B}$) at iteration 1 (Exploration) and 10 (RIC).

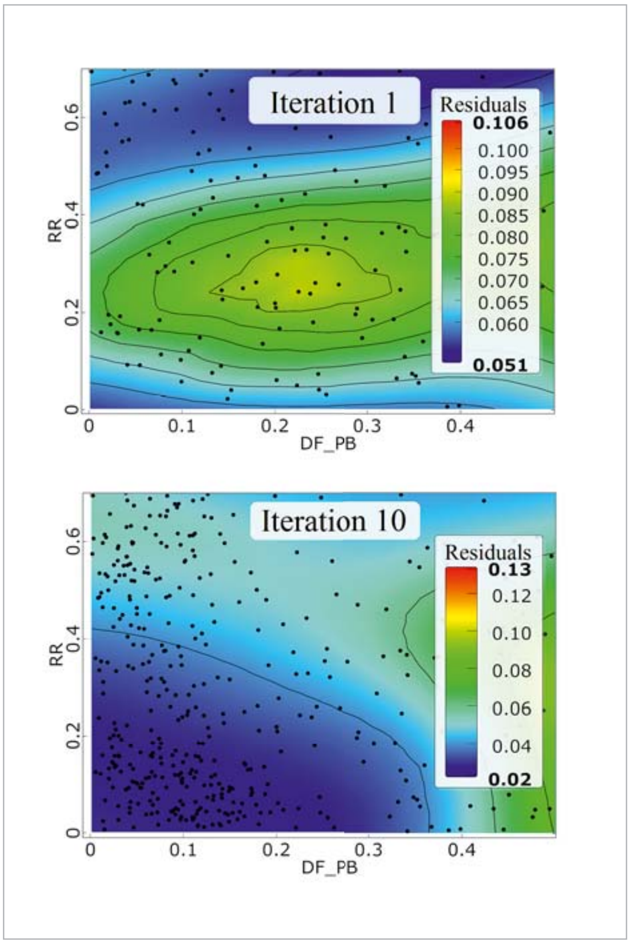

Fig. 6: 2-dimensional projection of the local residuals e of $\Delta\tau_{rg}$ for iteration 1 (exploration) and iteration 10 (RIC).

of $\Delta\tau_{rg}$. Fig. 6 shows the local residuals e of the metamodel in the same range as Fig. 5. We find that uncertainty is quite high at iteration 1, especially in the area of low predicted errors $\Delta\tau_{rg}$. This implies a bad estimate $\hat{\beta}$. After increasing the number of anchor points to more than twice the original count, at iteration 10, residuals were significantly lower, especially in the interesting areas of the metamodel.

Fig. 7 shows the relationship between the residuals e in regions of low predicted errors $\Delta\tau_{rg}$ and iteration number for the entire parameter space. Stagnation begins after iteration 3, which suggests that adding samples does not improve the metamodel anymore [16].

In the next step the minimum error min ($\Delta\tau_{rg}$) was determined on the metamodel with the NLPQL optimizer. The runtime was < 1 min. The metamodel was then validated at the supposed minimum x_{opt} according to Table 1, showing a very good match (Fig. 8). This confirms that the metamodel is indeed of high quality.

The optimized parameter set x_{opt} was then used for the two validation trials as shown in Table 1. The results are shown in Fig. 8. We find that the calibrated model exhibits a high fidelity in reproducing the experimental results. An overview over the accuracy of the DEM models is presented in Table 4.

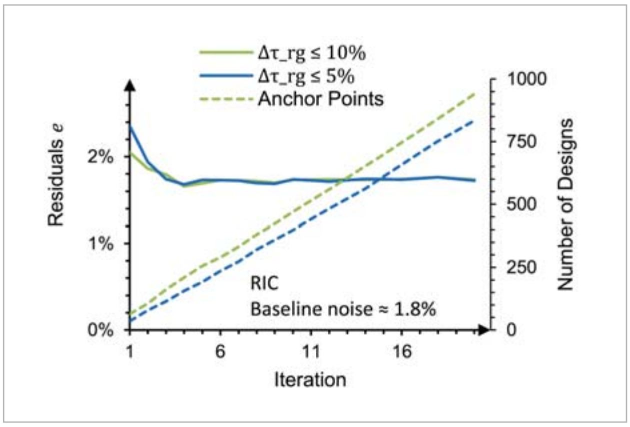

Figure 7: Residuals e of τ_{rg} for the areas of the metamodel with low predicted DEM model errors $\Delta\tau_{rg}$ over iterations (RIC). The respective number of iteration used to calculate the residuals are shown as dotted lines.

The entire calibration process was repeated with a constant initial condition (CIC) before the drop. The results are shown in Fig. 8. We obtain a nearly equally good result as in the case with the RIC. This suggests that the physical randomness was not crucial for the accuracy of the metamodel. This however could only be true for the particular initial condition chosen here.

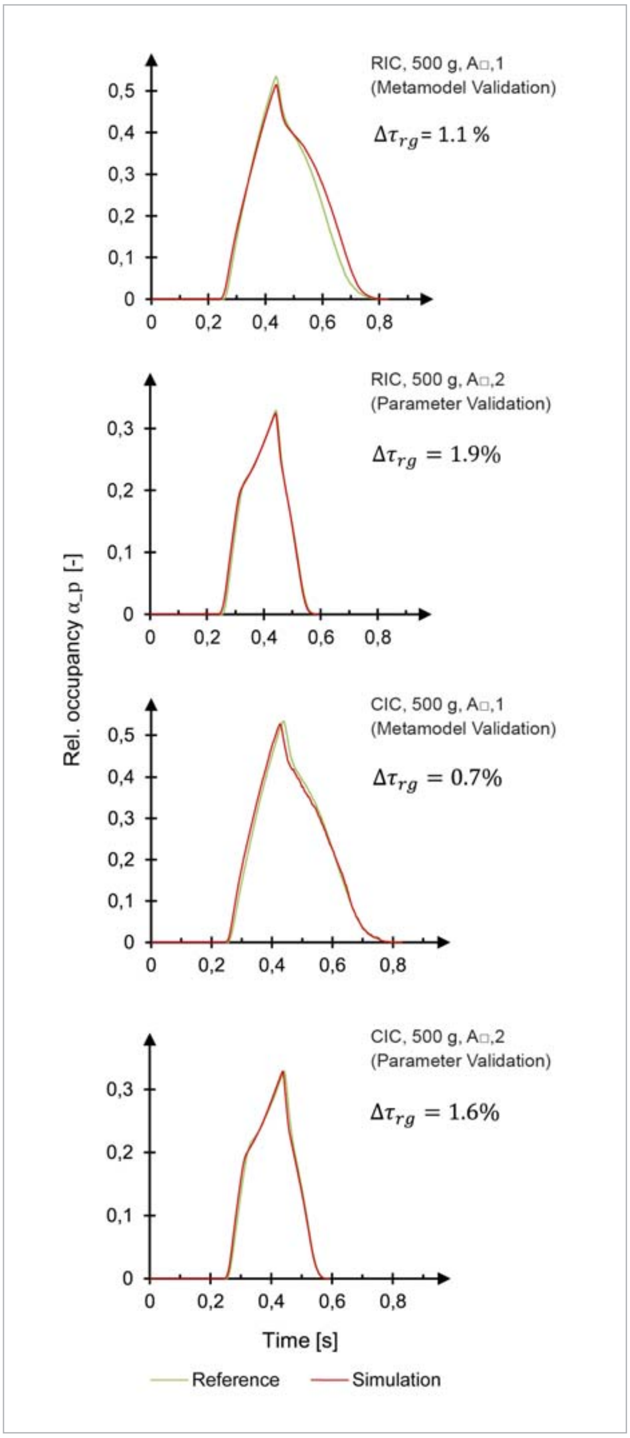

Fig. 8: Results of calibration in the drop test (RIC and CIC), validation of metamodel after optimization and parameter validation in the drop test with A□,2 > A□,1

m=20	Metamodel Validation	Parameter Validation		
		500 g, A□,1	500 g, A□,2	700 g, A□,1
Drop, RIC	$\Delta\tau_{rg}$=1.1%	-	$\Delta\tau_{rg}$=1.9%	$\Delta\tau_{rg}$<0.1%
Drop, CIC	$\Delta\tau_{rg}$=0.7%	-	$\Delta\tau_{rg}$=1.6%	$\Delta\tau_{rg}$=0.7%

Table 4: Actual error of τ_{rg} for metamodel validation and for the eventual calibrated parameters x for the random initial condition (RIC) and constant initial condition (CIC). Simulations were performed m=20 times and their results averaged

Conclusion

We found that the selected drop test is a suitable experimental approach for DEM model calibration, yielding low prediction errors of a maximum of 2%. The calibration was repeated without physical noise, which yielded an equally good result. This suggests the conclusion that physical noise is not relevant for the calibration, however it still needs to be proven whether this is true for all initial conditions or only some.

Author // St. Kirsch (Robert Bosch Packaging Technology B.V.)

References //

[1] O. R. Walton et al., "Viscosity, granular temperature, and stress calculations for shearing assemblies of inelastic, frictional disks", Journal of Rheology, 1986.

[2] S. Luding, "Collisions & Contacts Between Two Particles", Physics of Dry Granular Media, vol. 350, pp. 285-304, 1998.

[3] S. Kirsch et al., "Simulation of Vertical Filling Processes of Granular Foods for typical Retail Amounts", in 9th Conference Processing Machines and Packaging Technology, 2018.

[4] L. Benvenuti et al., "Identification of DEM simulation parameters by Artificial Neural Networks and bulk experiments", Powder Technology, vol. 291, pp. 456-465, 04 2016.

[5] C. J. Coetzee, "Review: Calibration of the discrete element method", Powder Technology, vol. 310, pp. 104-142, 04 2017.

[6] T. Gröger et al., "On the numerical calibration of discrete element models for the simulation of bulk solids", in 16th European Symposium on Computer Aided Process Engineering and 9th International Symposium on Process Systems Engineering, Elsevier BV, 2006, pp. 533-538.

[7] T. Shinbrot, "Granular chaos and mixing: Whirled in a grain of sand", Chaos, vol. 25, 09 2015.

[8] Y. Xu, et al., "Effects of material properties on granular flow in a silo using DEM simulation", Particulate Science and Technology, vol. 20, pp. 109-124, 04 2002.

[9] D. Markauskas et al., "Investigation of rice grain flow by multi-sphere particle model with rolling resistance", Granular Matter, vol. 13, pp. 143-148, 07 2010.

[10] C. González-Montellano et al., "Determination of the mechanical properties of maize grains and olives required for use in DEM simulations", Journal of Food Engineering, vol. 111, pp. 553-562, 08 2012.

[11] X. Huang, "Exploring critical-state behaviour using DEM", 2014.

[12] M. Frank et al., "Simulation-based optimization of geometry and motion of a vertical tubular bag machine", Sächsische Landesbibliothek, 03 2016.

[13] M. W. Johnstone, "Calibration of DEM models for granular materials using bulk physical tests", 2010.

[14] H. Q. Do et al., "A calibration framework for discrete element model parameters using genetic algorithms", Advanced Powder Technology, vol. 29, pp. 1393-1403, 06 2018.

[15] M. Rackl et al., "A methodical calibration procedure for discrete element models", Powder Technology, vol. 307, 02 2017.

[16] J. P. C. Kleijnen, "Simulation Optimization through Regression or Kriging Metamodels", Discussion Paper, 05 2017.

[17] T. Most et al., "Sensitivity analysis using the Metamodel of Optimal Prognosis", in Weimar Optimization and Stochastic Days, 2011.

[18] M. D. McKay et al., "A Comparison of three methods for selecting values of input variables in the analysis of output from a computer code", Technometrics, vol. 21, pp. 239-245, 05 1979.

[19] J. C. Helton et al., "Latin hypercube sampling and the propagation of uncertainty in analyses of complex systems", Reliability Engineering and System Safety, vol. 81, pp. 23-69, 2003.

[20] M. Rackl et al., "Efficient calibration of discrete element material model parameters using Latin hypercube sampling and kriging", in ECCOMAS Congress 2016 - Proceedings of the 7th European Congress on Computational Methods in Applied Sciences and Engineering, 2016.

[21] R. K. Rathore et al., "An Adaptive Approach for Single Objective Optimization", Int. Journal of Engineering Research and Applications, vol. 4, pp. 737-746, 02 2014.

[22] F. Jurecka, "Automated metamodeling for efficient multi-disciplinary optimisation of complex automotive structures", in 7th European LS-DYNA Conference, Salzburg, Austria, 2009.

[23] K. Schittkowski, "NLPQL: A fortran subroutine solving constrained nonlinear programming problems", Annals of Operations Research, vol. 5, pp. 485-500, Jun 1986.

[24] Y.-h. Dai et al., "A Sequential Quadratic Programming Algorithm with Non-Monotone Line Search", Pacific Journal of Optimization, vol. 4, 2008.

The full report "DEM Model Calibration for Vertical Filling: Selection of adequate Trials and Handling Randomness" is available on:
https://www.dynardo.de/fileadmin/Material_Dynardo/bibliothek/Optimierung_Sensitivitaet/Kirsch_2018_DEM_calibration.pdf

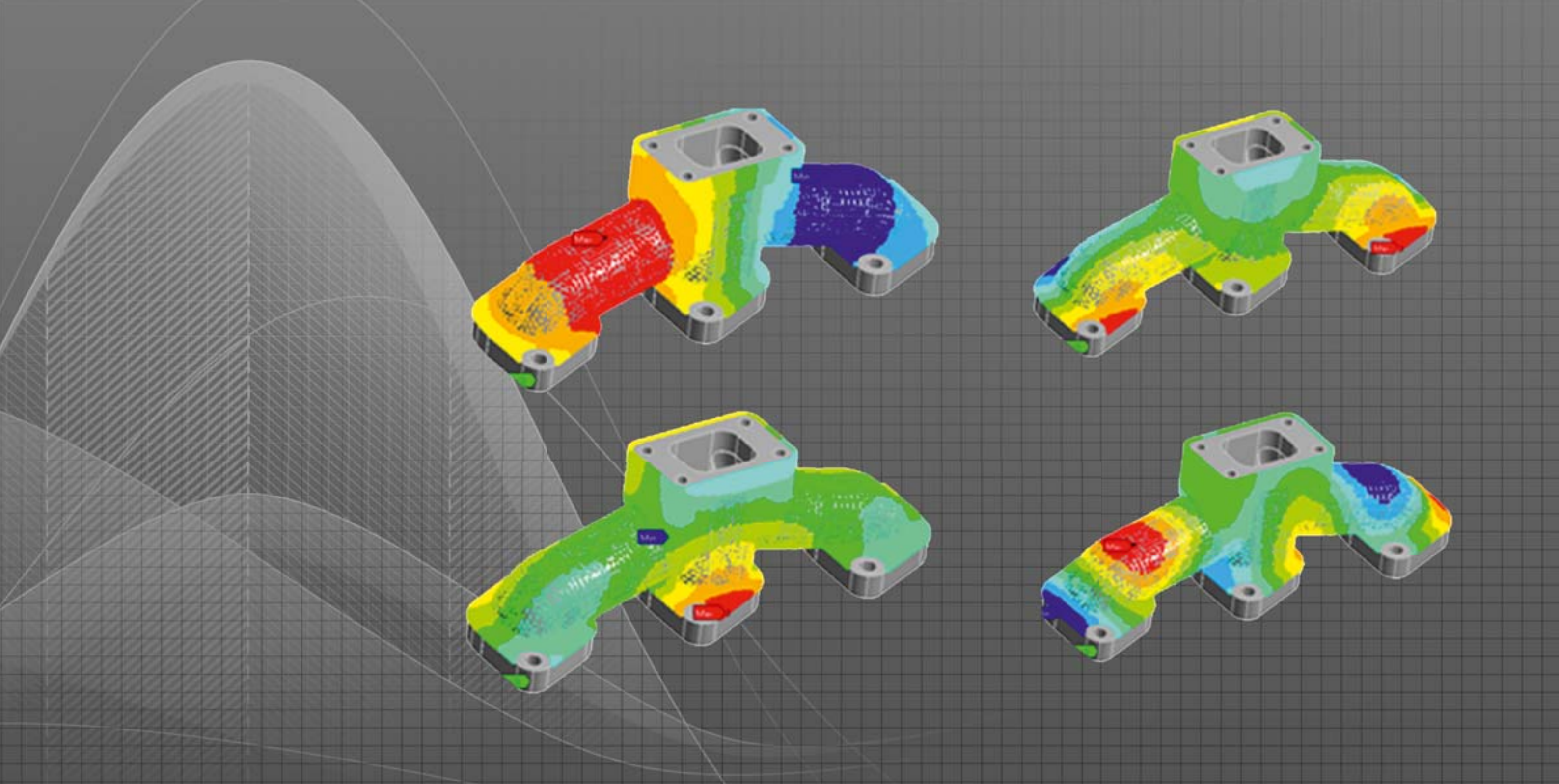

CASE STUDY // AUTOMOTIVE ENGINEERING

SENSITIVITY ANALYSIS OF THERMO-MECHANICAL FATIGUE LIFE OF AN EXHAUST MANIFOLD

ANSYS India conducted a reduced order model based sensitivity analysis of thermo-mechanical fatigue life of an exhaust manifold subjected to uncertainties in material, loading and manufacturing.

Introduction

Exhaust manifold components in the automotive industry are typically subjected to high thermo-mechanical cyclic load and prone to fatigue failure. Location of minimum life varies with mainly three factors – inaccurate determination of material model coefficients, thermo-mechanical load variation and manufacturing variability such as uneven thickness of the manifold wall because of the casting process. Manufacturing variability is random in nature and difficult to address through deterministic CAD model change and to be re-run as an entire simulation for life estimate of components. At the same time, a large number of prototype casting and testing incurs huge cost.

This article describes a model order reduction technique to quantify the spatially distributed manufacturing variability using random field shapes for component wall thickness variation combined with mesh morphing to produce different geometries. As the material yield points often could not be determined with confidence, field models are used to generate additional random parameters. Also, randomness of the peak cyclic temperature and corresponding convection film coefficients are represented by random input parameters. Minimum fatigue life and its location is identified from a quantile plot over the component surface. Finally, the sensitivity for the minimum fatigue life is estimated using a variance based sensitivity analysis. In the following two sections, material modeling and fatigue life estimation using crack tip opening displacement (CTOD) methods will be described briefly. Finally, a quantification of uncertainty will conclude the study.

Selection of Material Models

Selecting the right material for different parts of the component form is a critical element to design for thermo-mechanical fatigue. It is important to characterize how this material behaves when exposed to different loads and conditions. For material characterization, the usual procedure would be to capture through physical testing of coupons how the materials behave at different temperatures, strain ranges, strain rates, dwell periods, different phases between thermal and mechanical strain, environments, etc. Rate effects are dominant at temperatures higher than half the homologous temperature. Furthermore, isotropic work hardening is more dominant at lower temperatures.

The effect of strain rate is captured through a viscoplastic model, which essentially follows what is known as the over stress model. At very slow plastic strain rates, a characteristic of this model is to follow the rate independent plasticity. In this case, the stress is at the yield surface. The applied model has multiple layers and is able to capture the viscoplastic behavior at different stress levels.

Kinematic hardening captures the Baushinger effect, where the centre of the yield surface moves in response to plastic strains. At this centre, kinematic hardening represents the back stress in the system. In these alloys, this movement has a distinct non-linear behavior and, similar to work hardening, has a limiting surface to which the yield surface can move to. The implementation of the Chaboche model (Chaboche, 1989) (Chaboche, 1981) is able to capture these characteristics accurately. As an additional rate effect, the back stress, which manifests as self-equilibrated microscopic residual stresses (Lemitre & Chaboche, 1990) at grain boundaries, becomes diffused and released if kept at high temperatures for some time. This causes the centre of the yield surface to drop back to its initial original state over time. This drop follows a non-linear behavior and is a strong function of the back stress itself. This rate effect is captured by enabling the static recovery term (ANSYS Inc, 2018) in the Chaboche model. Since the material has been characterized, the next step is to study what does the component experience as it goes through the duty cycle. If reality is mimicked in total, it would take a very long period of physical time to solve this task potentially, which would not be practical. In industrial practice, therefore a representative cycle approach is applied. Essentially, this means to look at the experience of the component through a duty cycle somewhere during its life. Often this is conducted at mid-life cycle. Then life is calculated based on the damage that happens in this cycle.

Life Calculation

Methodology

In this study, fatigue life calculation is based on CTOD (Crack Tip Opening Distance). Typically, due to presence of high temperature, the amount of inelastic strain in the component is considerable. Due to a huge plastic zone ahead of it, the crack tip becomes blunt. As the load is increased, the blunting increases and, after a threshold value of stress, the blunt tip opens up, i.e. crack propagates. He et al (He et al, 1981) analytically calculated the expression for J-Integral, consisting of separate elastic and plastic parts, for penny shaped cracks.

Opposed to stress values, strain values are computed between two time points in the stabilized cycle load-step. The two time points are shown in Fig. 1. The TMF damage is determined from J-integral. From damage, the fatigue life is calculated.

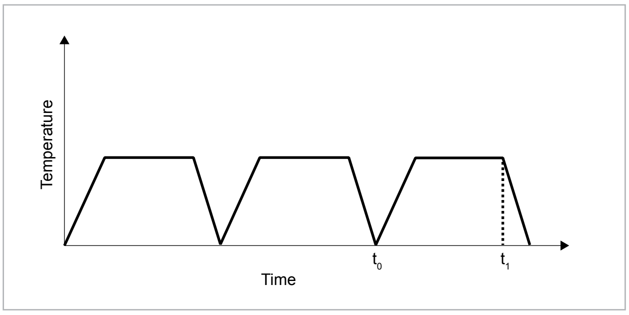

Fig. 1: Time points selected to find the difference in stress tensors

Life Calculation Results

During this study, the component was subjected to temperature cycling as shown in Fig. 2.

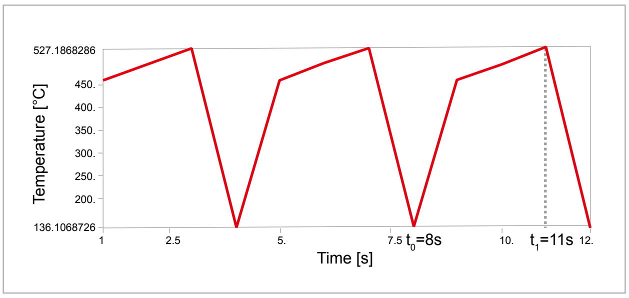

Fig. 2: Temperature profile

The plastic strains stabilized in the third cycle. The time points for calculating the stress and strain amplitudes were selected as t_0=8s and t_1=11s. From the stress and strain amplitudes, the damage was calculated for the stabilized cycle. The life was then calculated for each element.

While reporting life, the bolt locations were excluded from the model. Bolt locations mostly had high stress concentration and singularity as shown in Fig. 3. Also, the critical location based on the deformation pattern appeared at the bends.

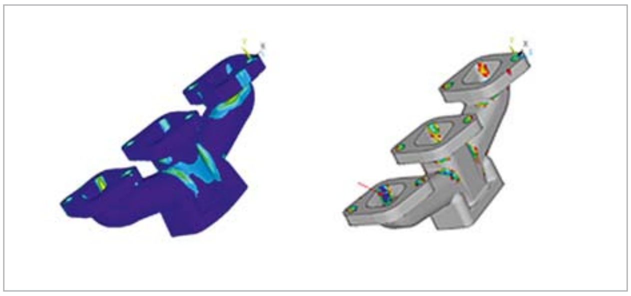

Figure 3: Plastic strain (left) and life plot (right)

Low life regions mostly appeared at bend. Further the life and strain plots showed 180-degree rotation symmetry. Afterwards, as described in the following section, a sensitivity analysis was performed to identify the critical input parameters responsible for minimum fatigue life.

Uncertainties in Exhaust Manifold Design

In this study, yield stresses at five temperature points (20, 300, 500, 550 and 6000C) were given a ±10% variation on the respective reference values. Additionally, the highest cyclic temperature was given a ±10% variation on the reference value of 6000C. A variation of ±10% was also considered for the convection film coefficient at the inner surface of the manifold. Manufacturing defects or nominal variation of the geometry from the casting process were accounted through a special morphing technique clubbed with statistical formulation of the spatially distributed randomness as described below. ANSYS optiSLang along with Statistics on Structures (SoS) was used to generate the random fields and to perform the sensitivity analysis as well as the uncertainty quantification.

Random Geometry Generation through Mesh Morphing

A synthetic random field parametric model, representing possible uncertainties in geometry, was generated on top of the nominal mesh of the idealized perfect geometry model. The outer surface of the exhaust manifold was provided as the surface mesh to be morphed using the synthetic random field model. To generate the synthetic random field for every surface nodal point, max/min normal movement was defined using a standard deviation value. An internal autocorrelation matrix based on the distance between nodes was solved in an eigenvalue analysis and its eigen shapes and related distribution of amplitudes were generated. Eigen shapes represent variation shapes (scatter shapes) of outer surface of the manifold as shown in Fig. 4. Positive and negative values within an Eigen shape indicate outward and inward normal movement of the node. A selection from the resulting Eigen shapes was used in the morphing process of the surface nodes. Each morphing shape together with mesh relaxation techniques was tested separately to ensure that the element Jacobian ratios were maintained for accuracy of the finite element solution. The first 14 shapes were used for the random field parametric model. They were able to explain any arbitrary variation of the manifold outer surface representing 95% of total possible surface variation. To generate imperfect surfaces, the shapes were multiplied with random amplitudes and combined algebraically so that at every node the target input standard deviation value was not exceeded.

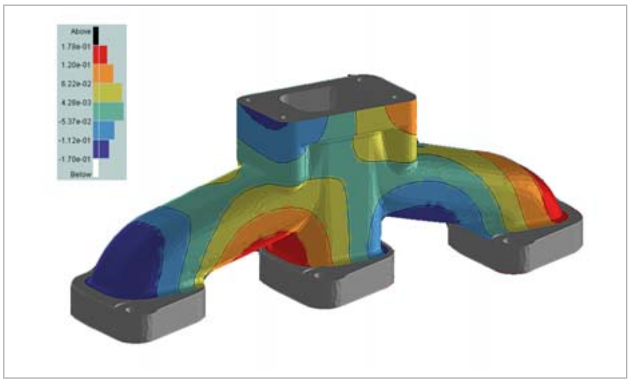

Fig. 4: Eigen shape contour showing normal movement of node

Sensitivity Analysis

Using the 14 random amplitudes of the Eigen shapes and additional random parameters, in total 21 uncertain parameters were considered and their effect on the fatigue life was studied using a sensitivity analysis plus uncertainty quantification. A Latin Hypercube Sampling scheme was used for the Design of Experiment and 95 design point results were accomplished. The location of the minimum value of life was identified from a quantile plot over the manifold surface of 95%, i.e., there was 5% probability of exceeding the plotted minimum life values. Five such critical hot spot locations were identified where the life values are low. They are shown in the quantile plot Fig. 5.

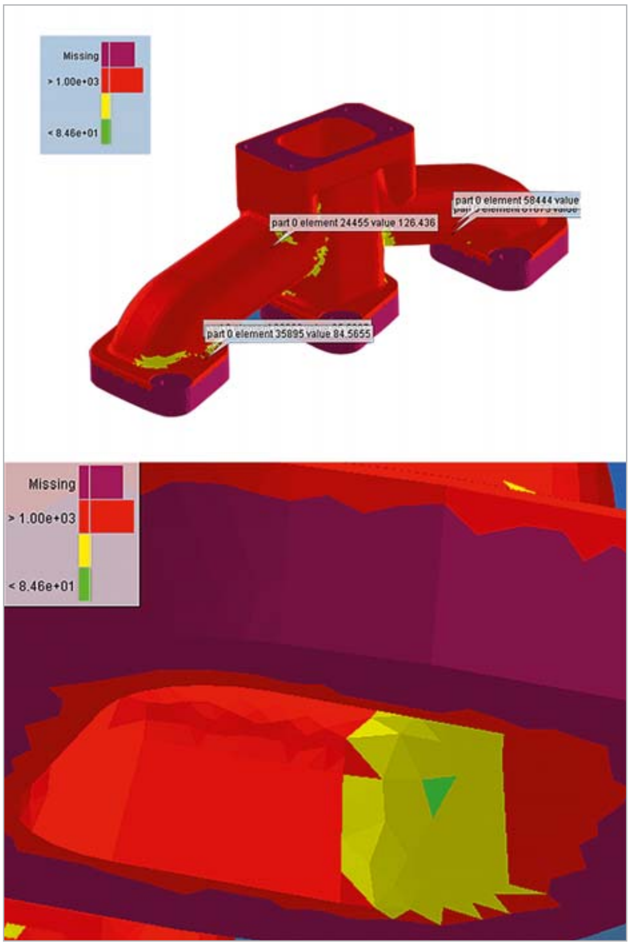

Fig. 5: 95% quantile plot for fatigue life

Hot Spot Sensitivity

For the above mentioned five locations, a sensitivity analysis based on the 95 design points was performed. The sensitivity of minimum life is plotted in Fig. 6 for the location shown in Fig. 5. The peak cyclic temperature and film coefficient were the most influential input parameters and followed by four geometry scatter shapes, which had the largest influence on the variability of the life estimate.

Fig. 7 shows the distribution of change in thickness of walls for the sensitive shapes 2, 10, 11 and 13. It could be observed that all the above shapes were changing the thickness at the minimum life location shown in Fig. 5.

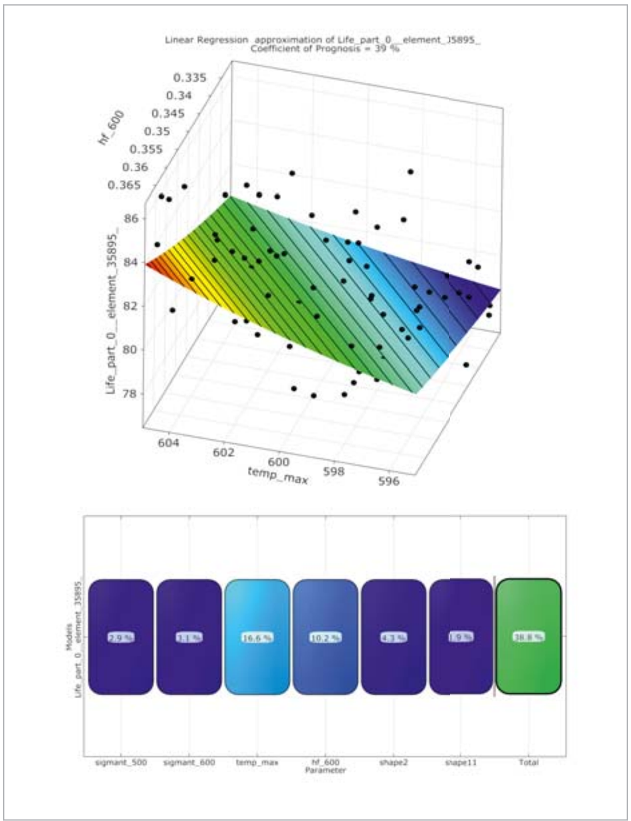

Fig. 6: Metamodel of Optimal Prognosis for minimum life location

The forecast quality of the variability of minimum life on the response surface was only around 60% as shown in Fig. 6. The reason can be attributed to multiple facts. Firstly, 95 runs may not be sufficient for the sensitivity analysis with 21 parameters. It may require some more runs to improve the forecast quality of the metamodel. Secondly, linear tetrahedral coarse mesh was used for the acceleration of the study. This might introduce locking in the mesh and noise for the response quantities, which could lead to lower prediction quality. Thirdly, the metamodels were generated for five positions of expected minimums. In case the minimum locations are moving as a result of input variability, the extraction process may add the same additional noise to the results.

CONCLUSION

In this study, a generic uncertainty quantification approach is presented to counter the randomness in nonlinear material modeling, thermo-mechanical loading and manufacturing tolerance altogether. A quantile plot based assessment of the minimum crack location and the corresponding sensitivity analysis helped to identify the important variables, which can change the location of cracks and often make it vulnerable in-service life. The uncertainty quantification in life was performed on the base of the Latin Hypercube sampling.

Authors //

P. Som, P. Andrade, K. Kartikeya, R. Masal (ANSYS India)

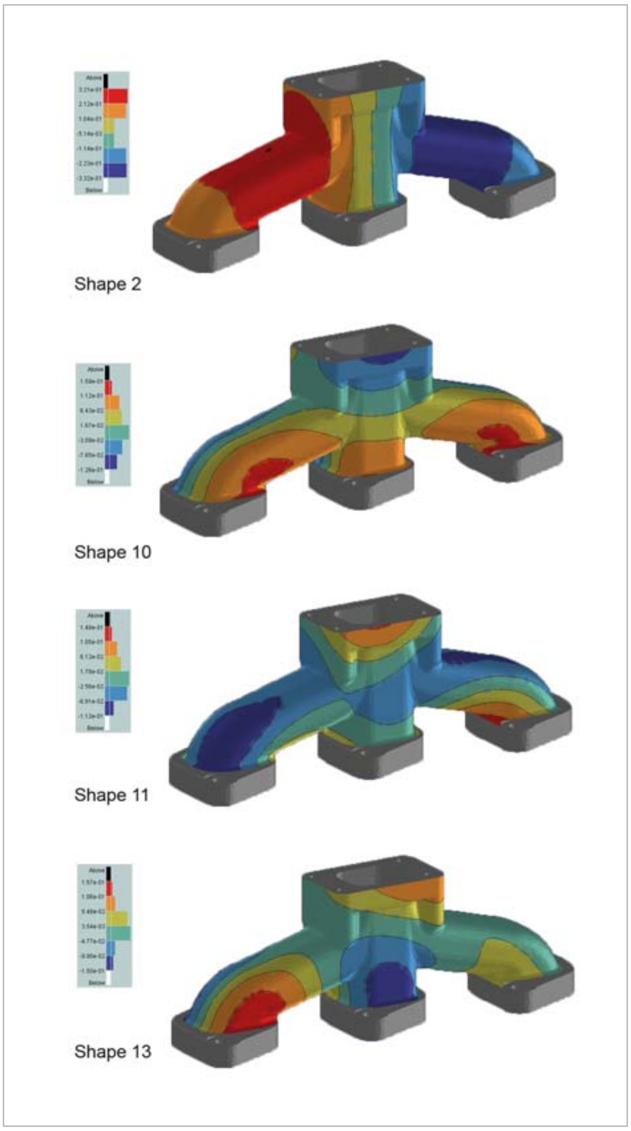

Fig. 6: Metamodel of Optimal Prognosis for minimum life location

Acknowledgement //

We are thankful to Dr. Sebastian Wolff from Dynardo Austria for his help.

References //

ANSYS, Inc. (2018), Theory Reference for ANSYS 19.0, Canonsburg, PA.

Chaboche, J. L. (1989) "Constitutive Equations for Cyclic Plasticity and Cyclic Viscoplasticity." International Journal of Plasticity. 5.3: 247-302.

Chaboche, J. L. (1991) "On Some Modifications of Kinematic Hardening to Improve the Description of Ratchetting Effects." International Journal of Plasticity. 7.7: 661-678.

Lemaitre J. and Chaboche J. L. (1990) "Mechanics of solid materials" Cambridge University Press

Hartrott, P. v., Seifert, T., & Dopps, S. (2014) TMF Life Prediction of High Temperature Components Made of Cast Iron HiSiMo: Part I: Uniaxial Tests and Fatigue Life Model. SAE International, 7(2), 439-45.

He, M. Y., & Hutchinson, J. W. (1981), The Penny-Shaped Crack and the Plane Strain Crack in a Infinite Body of Power Law Material. Journal of Applied Mechanics, 48, 830-40.

Metzger, M., & Seifert, T (2012). A Mechanism-Based Model for LCF/HCF and TMF/HCF Life Prediction: Multiaxial Formulation, Finite-Element Implementation and Application to Cast Iron. TECHNISCHE MECHANIK, 32, 435-45.

Seifert, T., Hazime, R., & Dropps, S (2014). TMF Life Prediction of High Temperature Components Made of Cast Iron HiSiMo: Part II: Multiaxial Implementation and Component. SAE International, 7(2).

Statistics on Structures (SOS), 3.3.3, (2018), Theory Documentation, Dynardo Gmbh

CUSTOMER STORY // AUTOMOTIVE ENGINEERING

COST AND FUNCTION OPTIMIZATION APPLIED TO A PROPORTIONAL SOLENOID

The application of optiSLang supports CAE-processes of cost and function optimization to create, compare and evaluate different competitive design variants of solenoids used for the control of automatic transmissions.

Introduction

Dilemma of the Product Development

Cost as well as function of a product are decisively influenced by its requirements, customer benefits and, especially, by its design. There are different development approaches to reduce the cost and to optimize the function of products, which differ in scope, potential of influence and required time for either new development or an extension of a new variant or a ratio project.

In addition to a reduction of the product costs, these approaches also lead to a launch of new products and technical innovations in shorter time, with the goals of high quality and attractive prices. The greatest potential for influencing costs and functions is in the time of product planning and development at the beginning of a product realization like shown in Fig. 1. The design, development and production planning departments influence cost and function of a product with approximately 90 % by a simultaneous cost share of about 9 % as given in Ehrlenspiel et. al. (2014). Due to these facts, a very close networking of technical-scientific and cost accounting aspects in these three departments is necessary.

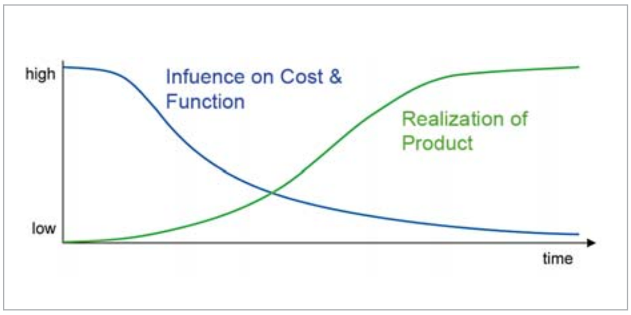

Fig. 1: Dilemma of the product development in reference to Ehrlenspiel et. al. (2014)

The challenge in designing products is to seek an optimal combination of function and cost fulfillment without the knowledge where to search exactly. One reason for this dilemma can be different and contradictory needs of customers and the number of possible solutions. In order to determine the cost and functional optimum, several component topologies with different materials, manufacturing processes, geometric parameters and tolerances would have to be developed, designed and compared to each other.

Even a simple comparison of different screw connections, which can be interpreted as different product topologies, shows the complexity cost correlation only in terms of different relative costs.

Performing such a detailed study as shown in Fig. 2 for all components of a product will require a large number of samples, development time and costs. No company can afford such an effort due to the cost and time pressure referred by Reischl (2000). In practice, therefore only a few detailed solutions are compared for example on the basis of a morphological box and a subsequent pairwise comparison or similar development methods. The resulting product costs are either estimated using different methods or calculated with the appropriate effort as mentioned e.g. in Pahl et. al. (2007).

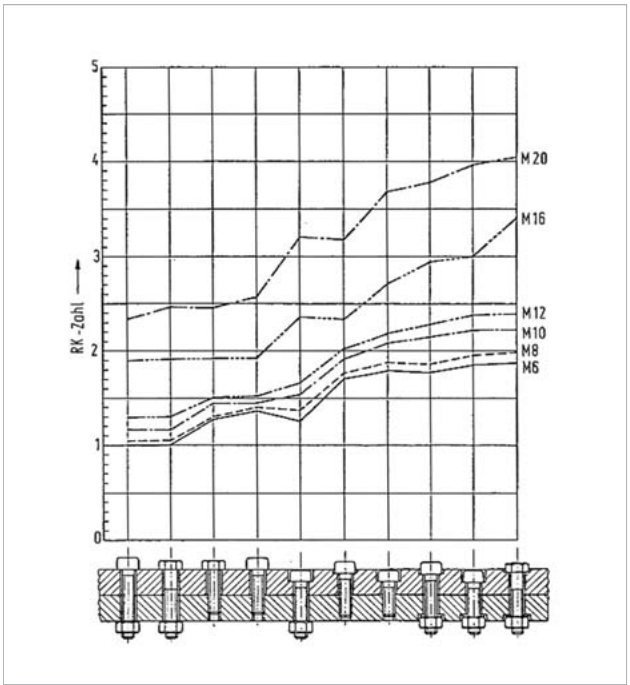

Fig. 2: Influence of the component topology on the costs using the example of relative costs for screw connections as shown in Naefe (2012)

Innovation Hypothesis

This detailed problem description clearly shows the complexity and comprehensiveness of a cost and function optimization. It also becomes obvious that there is a great potential in creating such a methodology. Here, the basic focus is to produce a variety of variants with different component topologies in a short time for the analyses of their functions and costs. Finally, this evaluation enables a faster development of competitive and innovative products.

The actual state of the art is a purely functional optimization based on a parameterized product model and a defined workflow as shown in Fig. 3. Computer-aided optimization software, e.g. Dynardo's optiSLang, was used as shown in Schwarz (2018). New design variants are generated by using an evolutionary algorithm, which varies geometrical parameters like diameter and length measures within specified limits. Here, the functional characteristics are determined by simulation and are evaluated in accordance with the target values and constraints for each design. Due to the optimization logic, which is contained in the algorithm and the objective functions, a so-called Pareto diagram is created as it can be seen in the middle of Fig. 3 for two technical objectives.

Part of the presented research work is to determine the cost for each generated design and to declare and optimize this value as a target. In this article, such an extension is described for the first time. Consequently, the potential solution space is extended by an economical dimension as shown on the right side of Fig. 3.

Linear Force Solenoid for Automated Transmissions

The method is developed by using the example of a proportional solenoid, as depicted in Fig. 4 (see next page). This solenoid is used to control automatic transmissions. Usually, such a solenoid is operated at a maximum of 1,2 A and generates

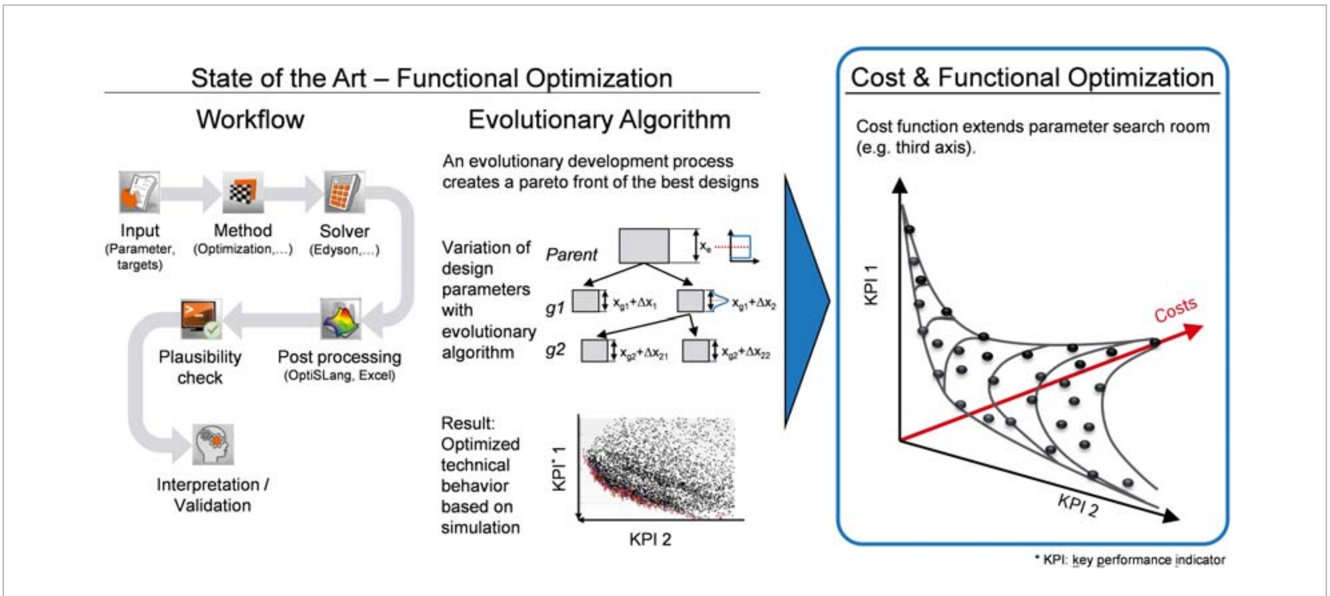

Fig. 3: State of the art and innovation hypothesis

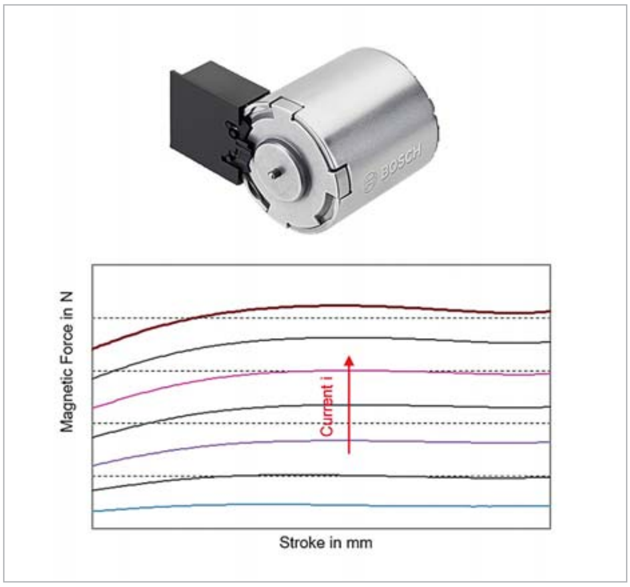

Fig. 4: Linear Force Solenoid with its characteristic curve of magnetic force stroke

a magnetic force of up to 25 N. The customer specifies the characteristic curve of the magnetic force stroke for different current levels as shown in Fig. 4. Typical customer specifications are particular forces and slope gradients at given stroke positions. For the solenoid used in this investigation, a function optimization like illustrated in Fig. 3 (see previous page) has already been available. Due to the large number of pieces, the product is very well suited for an extension of the function optimization to a cost and function optimization.

Requirements to set up a Cost and Function Optimization

The prerequisites for the optimization of costs and functions are, on the one hand, the determination of the component cost and, on the other hand, the expansion of the variables for effective cost optimization. In each case, a differentiable cost surcharge calculation is performed to determine the component costs. In addition to the material costs based on geometrical parameters, this approach also includes the costs for the added value as shown in Fig. 5. With the information on the production process chains, the respective cycle times and the machine hourly rates must be calculated. The more accurate the underlying data base, the more accurate is the calculation. In this study, the data sources are taken from purchasing, manufacturing and cost experts.

As already mentioned, not only the previous geometric design parameters are varied for the generation of new designs, but also the materials and the associated manufacturing technologies, as well as tolerances and topologies of the individual components. These extensions of the variables have an impact on the cost calculation. As a result, the number of possible variants and combinations increases and correlations become apparent.

Workflow

Derived from the requirements for a cost and function optimization, a workflow is set up, which not only varies geometric design parameters but also materials by its material number. Based on the selected material, the material parameters for the magnetic force simulation are automatically adjusted and the manufacturing processes for the cost calculation are updated, see Fig. 6.

Furthermore, differently designed simulation models for the proportional magnet are created by topology variables. The topology variable controls the selection of a bill of material (BOM) from a large number of already predefined BOMs. They describe possible solenoid structures. Based on the selected BOM, the geometry model is assembled in a Python script and Gmsh does the meshing according to Geuzaine (2009). At the same time, the tolerance classes of

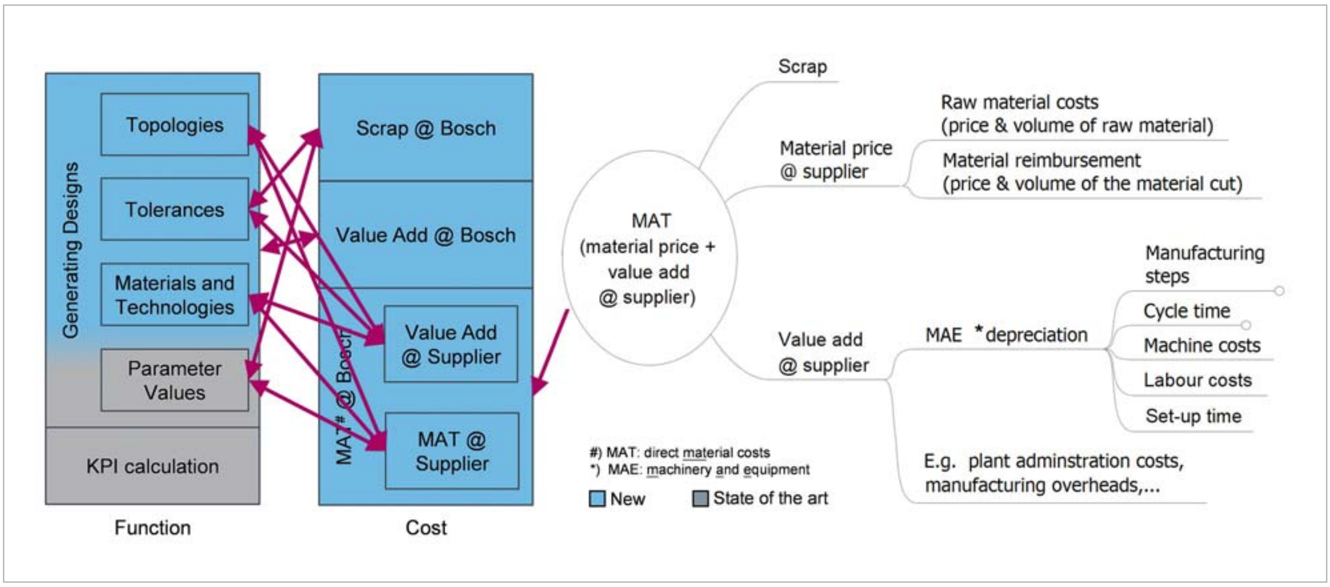

Fig. 5: Requirements to set up a cost and function optimization

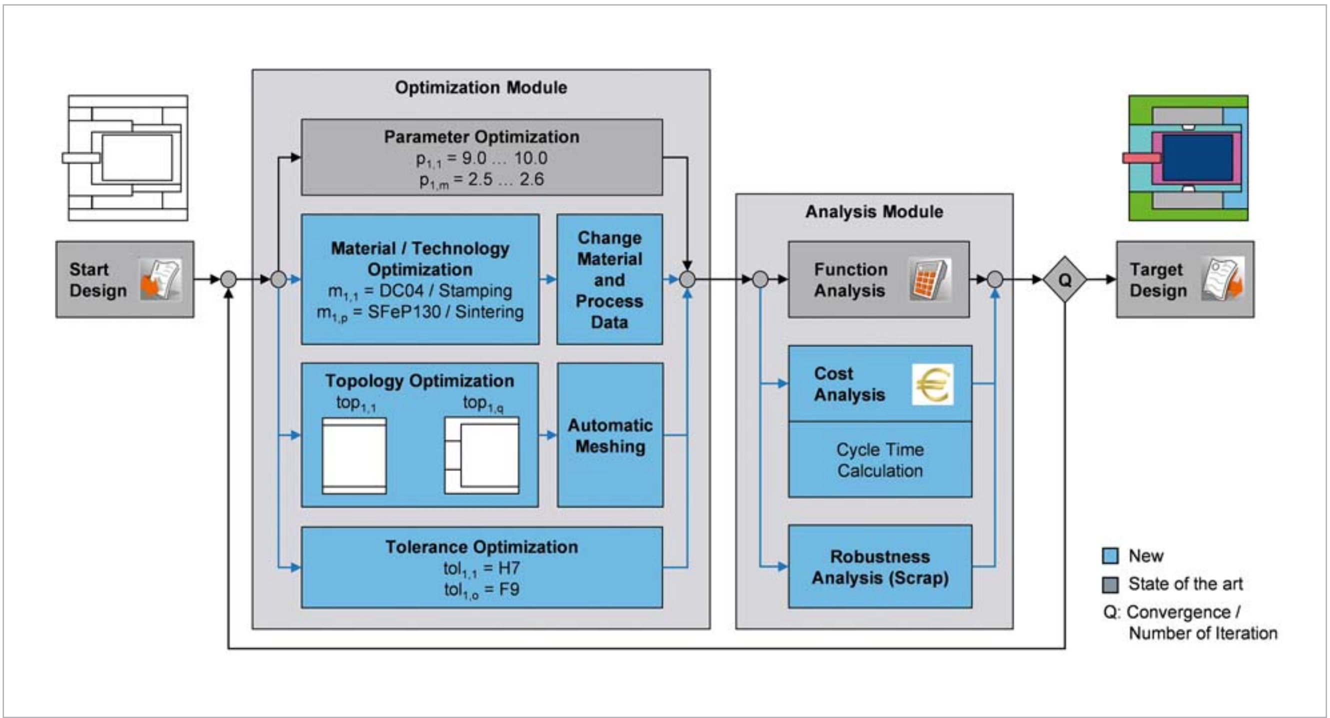

Fig. 6: Schematic representation of the cost and function workflow

the selected geometrical design parameters are varied via discrete variables. The tolerance class has an impact on the manufacturing process chains as well as on the integrated robustness analysis (for more details see chapter Tolerance Optimization).

As a starting point for the optimization either one or more start designs can be defined. Ideally, this start design is determined by a previous sensitivity analysis. Based on the start design, the listed variables, such as geometric design parameters, materials, topologies and tolerances, can be considered, varied or optimized either individually or in any possible combination in the optimization module. After the optimization module, the so-called analysis module is processed. This analysis module includes the electromagnetic simulation, the Python based cost calculation and the robustness analysis. The process repeats itself until a maximum number of designs has been generated or a convergence with the optimization goals has been achieved.

The realized workflow generates a Metamodel of Optimal Prognosis (MOP), see Most (2008), which is based on a sensitivity study covering 4000 designs using Latin Hyper Cube Sampling, see Fig. 7. The MOP replaces the solver call for the function determination in the optimization as well as in the integrated robustness analysis. While a solver call

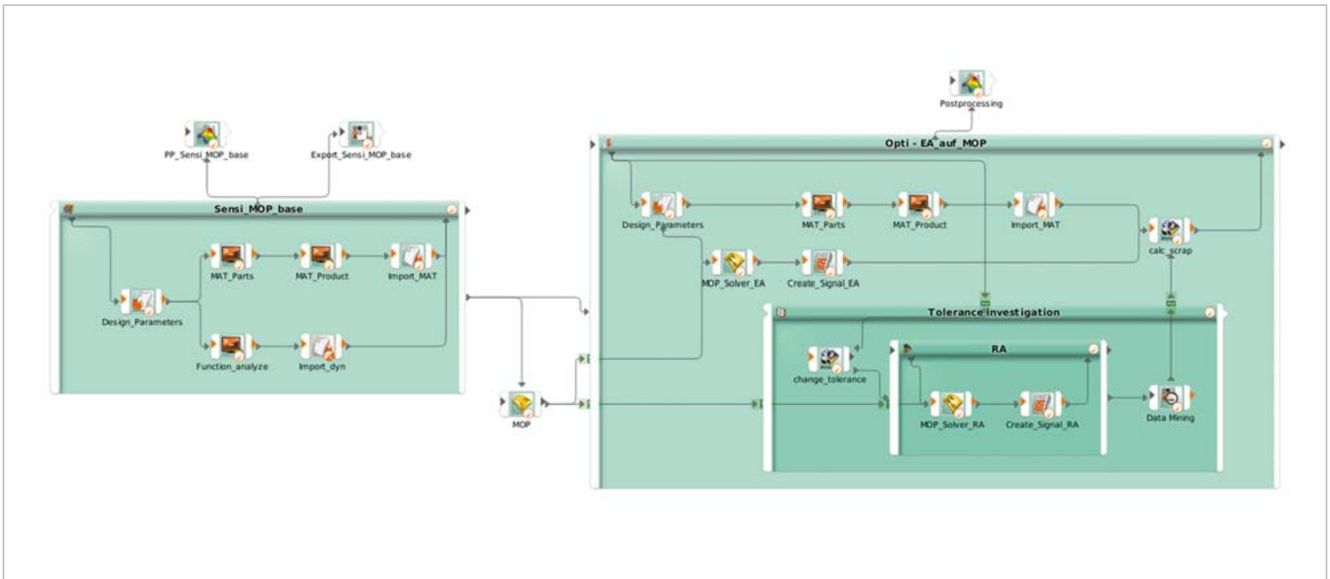

Fig. 7: Realized workflow in optiSLang

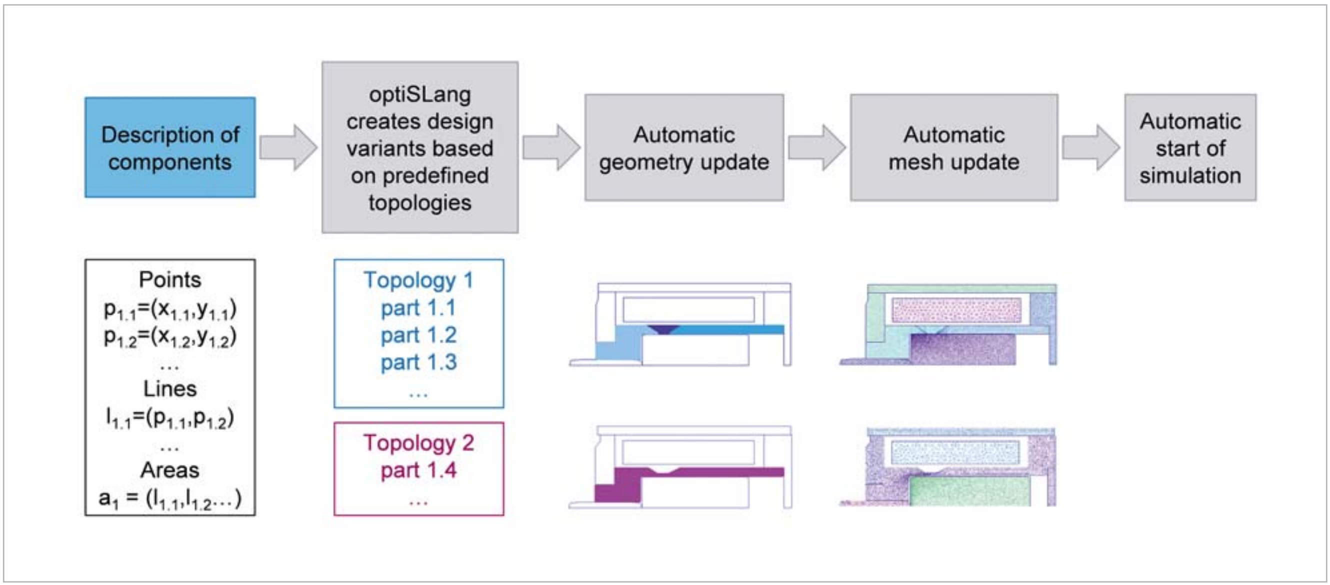

Fig. 8: Workflow of the topology optimization in detail

requires approximately 5 minutes the MOP produces an equivalent result instantaneously. Thus, replacing the solver call with MOP speeds up the optimization drastically. Using a Python script, the robustness analysis distributions are automatically calculated based on the generated designs. A data mining node extracts the distributions to check and pass on the relevant KPI like scrap-rate to the subsequent cost node.

Topology Optimization

All components are described upfront of an investigation by simple specification of the x, y coordinates, line definition and area assignment as shown in Fig. 8 on the left side. As already mentioned, the component descriptions are transferred into a geometry script by means of a Python script based on an already predefined bill of materials. This geometry script describes a design of which the simulation mesh is automatically generated with the use of Gmsh. The electromagnetic simulation starts as soon as this simulation model is available.

A first example shows the influence of two different geometries of the so-called pole tube, as they are highlighted in blue and pink in the center of Fig. 8. With the pole tube, the characteristic magnetic force-stroke curve of the proportional solenoid can be formed and also the armature is guided in it. The two considered topologies of the pole tube differ such that topology 1 (blue) consists of a three-part pole tube, whereas in topology 2 (pink), a one-piece pole tube is used. In this example, not only the topology but also the materials and geometrical parameters were varied.

When looking at the results in Fig. 9, two different solution spaces are recognizable, which basically depend on the topology. The solutions of topology 1 tend to be more expensive than the topology 2 due to the larger number of individual parts and the associated higher number of production steps. Nevertheless, its technical behavior is better due to its complete magnetic separation as described in Kallenbach et. al. (2012). In the end, a smaller deviation of the characteristic curve from the customer specification can be achieved.

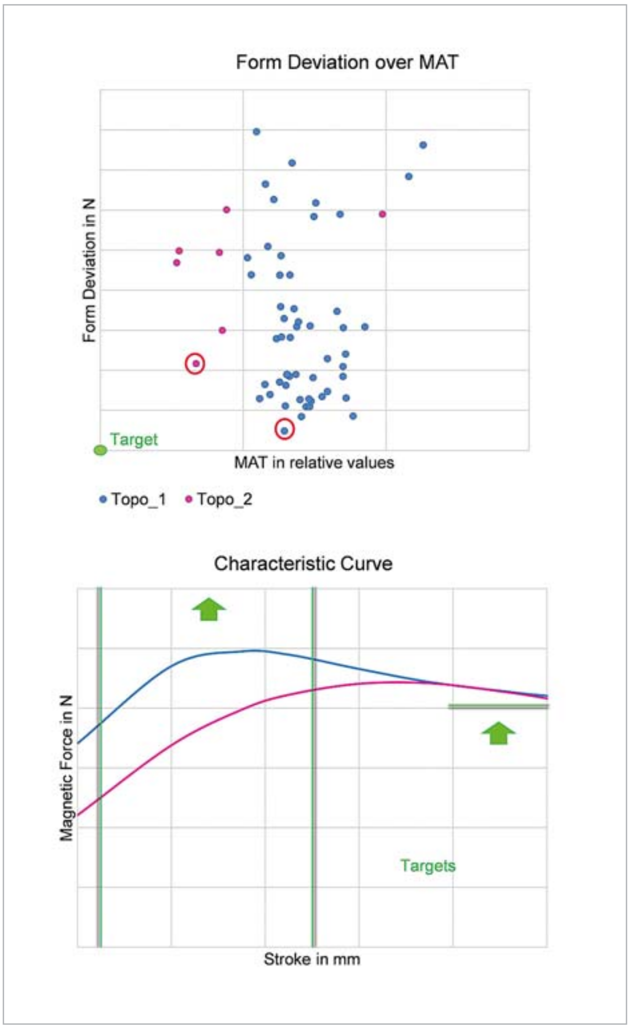

Fig. 9: First results of the topology optimization

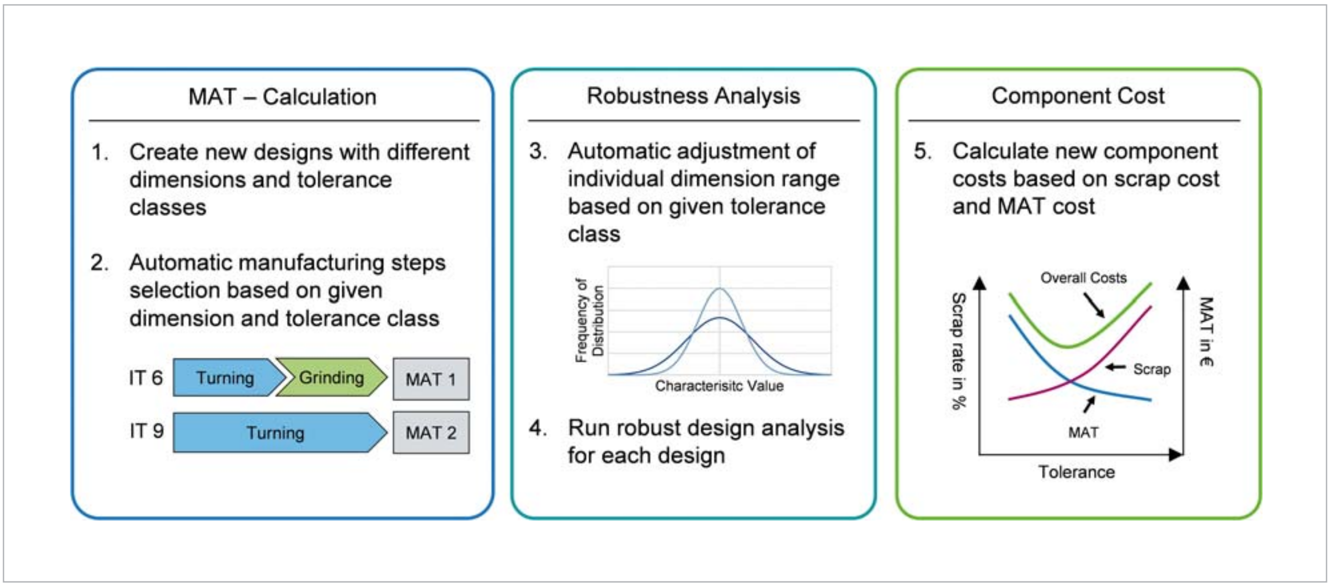

Fig. 10: Details of the tolerance optimization

The functional influence of a complete magnetic separation can be clearly seen by taking a closer look at the magnetic force-stroke curves. At the beginning of the stroke range, the magnetic force of the topology 1 is higher in contrast to topology 2, see the bottom diagram in Fig. 9. Due to the optimization criterion to maximize the force in this stroke range, the optimization algorithm favors the topology 1 as opposed to topology 2. Therefore, several designs are generated with topology 1. The boundary condition of not undercutting a certain force level at the end of the stroke range is achievable with both topologies.

Tolerance Optimization

In addition to the topology optimization, the newly developed method makes it possible to vary the tolerance classes and, consequently, also the standard deviation of individual geometrical design parameters in order to determine their influence on costs and function. By means of an integrated robustness evaluation in the analysis module, the variance of the design variants is automatically examined based on 50 further design variants, which scatter within the selected tolerance.

With the robustness analysis, it is therefore possible to produce a statement about the expected scrap of a design variant in form of an additional cost point, see Fig. 10. In addition, depending on the selected tolerance, a predefined manufacturing process chain for the production of this design is chosen, which influences the cost calculation. For example, for a very small tolerance class, a grinding process is required in addition to a turning process, see left side in Fig. 10.

In a first application of the tolerance optimization, the tolerance of a parameter, materials and geometric parameters are varied for one predefined topology. As shown in the upper diagram in Fig. 11, there are blue highlighted solutions with nominal tolerance. In addition, the optimization algorithm has also selected variants with a tighter tolerance class, which, as expected, have a higher MAT+Scrap value due to the more extensive and possibly more complex

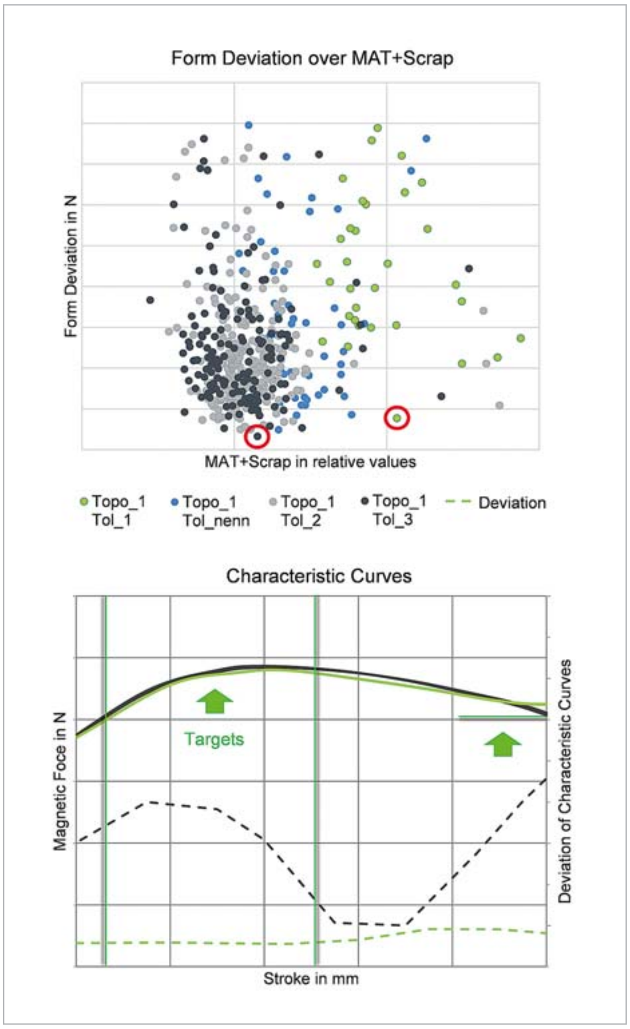

Fig. 11: First results of the tolerance optimization

production. In contrast, the design variants with larger tolerances tend to be more cost effective.

The comparison of the characteristic curve spread over the stroke range is interesting, as shown in the lower diagram in Fig. 11*. Here, the influence of the tolerance on the function is clearly recognizable and with it the justification of the different costs. Within the additional 50 designs along the entire stroke, the variant with the tighter tolerance (green lines in Fig. 11*) has a significantly lower dispersion (dotted green line in Fig. 11*) compared to the variant with the larger tolerance class (grey lines and dotted grey line in Fig. 11*). According to the simulation, this functional difference is associated with up to 12 % higher MAT. If the higher dispersion is acceptable for the customer, the preferred design should be one with an larger tolerance class. | * see previous page

Conclusion

For the first time, the developed workflow offers the opportunity to carry out an extensive cost and functional optimization. In this computer-aided simulation methodology, different materials, tolerances as well as component topologies are considered in addition to the well-established geometric design parameters. As a result, a variety of very different design variants are generated in a short time and a statement as well as the relationships in a technical and economic point of view can be derived. Due to a parallelization of the cost and functional analysis, this additional function does not contribute to increase the simulation time.

Authors//

M.Sc. A. Fuchs, Dr.-Ing. Ch. Ott, Dipl.-Ing. J. Bauer (Robert Bosch GmbH) / Prof. Dr.-Ing. F. Mantwill (Helmut-Schmidt-Universität/Universität der Bundeswehr Hamburg)

References //

EHRLENSPIEL, K., KIEWERT, A., LINDEMANN, U., MÖRTL, M.: Kostengünstig Entwickeln und Kosntruieren: Kostenmanagement bei der integrierten Produktentwicklung. 7. Auflage. Berlin: Springer-Verlag, 2014.

GEUZAINE, C.; REMACLE, J.-F.: Gmsh: a three-dimensional finite element mesh generator with built-in pre- and post-processing facilities. In: International Journal for Numerical Methods in Engineering 79 (11), PP. 1309-1331, 2009.

KALLENBACH, E., EICK, R., QUENDT, P., STRÖHLA, T., FEINDT, K., KALLENBACH, M., RADLER, O.: Elektromagnete – Grundlagen, Berechnung, Entwurf und Anwendung. 4. Auflage. Wiesbaden: Vieweg+Teubner Verlag, 2012

MOST, T., WILL, J.: Metamodel of Optimal Prognosis – an automatic approach of variable reduction and optimal metamodel selection. In: Proceedings 5th WOST 2008, Weimar, Germany, 2008

NAEFE, P.: Einführung in das Methodische Konstruieren. 2. Auflage. Aachen: Springer-Vieweg Verlag, 2012

PAHL, G., BEITZ, W., FELDHUSEN, J., GROTE, K.-H.: Konstruktionslehre – Grundlagen erfolgreicher Produktentwicklung, Methoden und Anwendung. 7. Auflage. Belin: Springer-Verlag, 2007

REISCHL, C.: Simulation von Produktkosten in der Entwicklungsphase. Technische Universität München, PhD thesis, 2000

SCHWARZ, H.: CAE-Software optiSLang. In: Product brochure optiSLang. Weimar, Germany, July 2018

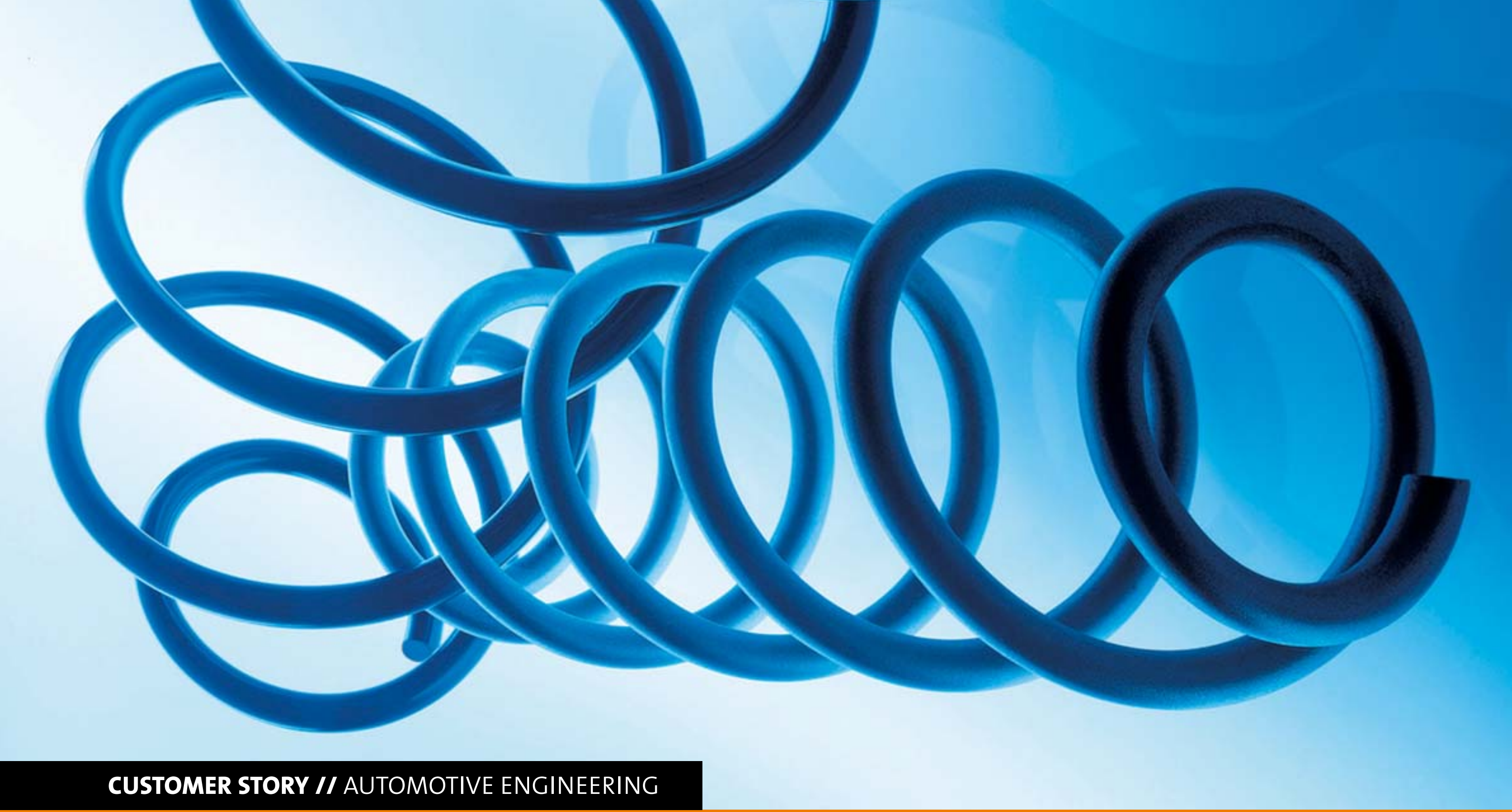

CUSTOMER STORY // AUTOMOTIVE ENGINEERING

AUTOMATED DESIGN AND OPTIMIZATION OF SUSPENSION COIL SPRINGS

At Mubea, FEA methods and optiSLang are applied for an automated design of coil springs with subsequent optimization procedure to fulfill all boundary conditions and lifetime requirements.

Introduction

The Mubea Group is a world leading manufacturer of complex automotive components that reduce vehicle weight and contribute to an improved environmental performance by reduced CO_2 emission. Suspension components represent a large proportion of the company's portfolio and revenue. The chassis components also include coil springs, which will be explained in the following.

Task of a suspension coil spring

The current density of traffic requires motor vehicles that are safe and comfortable to allow the driver to concentrate fully on the traffic during short and long distance rides. Therefore, not only intuitive designs, manageability, cost-effectiveness and fault-free operation, but also the demands for a high level of comfort and driving safety are of central importance.

The fulfillment of these requirements call for the involvement of resilient and damping components between the chassis and the vehicle body. On the one hand, these components must largely absorb road-induced impacts and vibrations and, on the other hand, must consistently ensure sufficient traction control of the wheels.

Helical compression springs as resilient components are particularly suitable because:

- their compact design enables a space-saving installation in subframes or on wishbones
- they can be combined with the damper to a unit (simple strut and McPherson strut)
- they show linear or even progressive characteristics
- their production is economical and inexpensive
- their operation is practically maintenance-free

In today's automobiles, in addition to the helical compression springs, often stabilizers are installed for supporting both one-sided and double-sided deflection of the wheels. Stabilizers essentially serve to reduce the rolling of the vehicle body when cornering, while helical compression springs primarily ensure a proper pitch response and ground clearance of the body.

Types of force transmission

For the positioning and force transmission, the design of the spring end coils are of crucial importance. Coil springs are usually installed inside or outside of their struts with

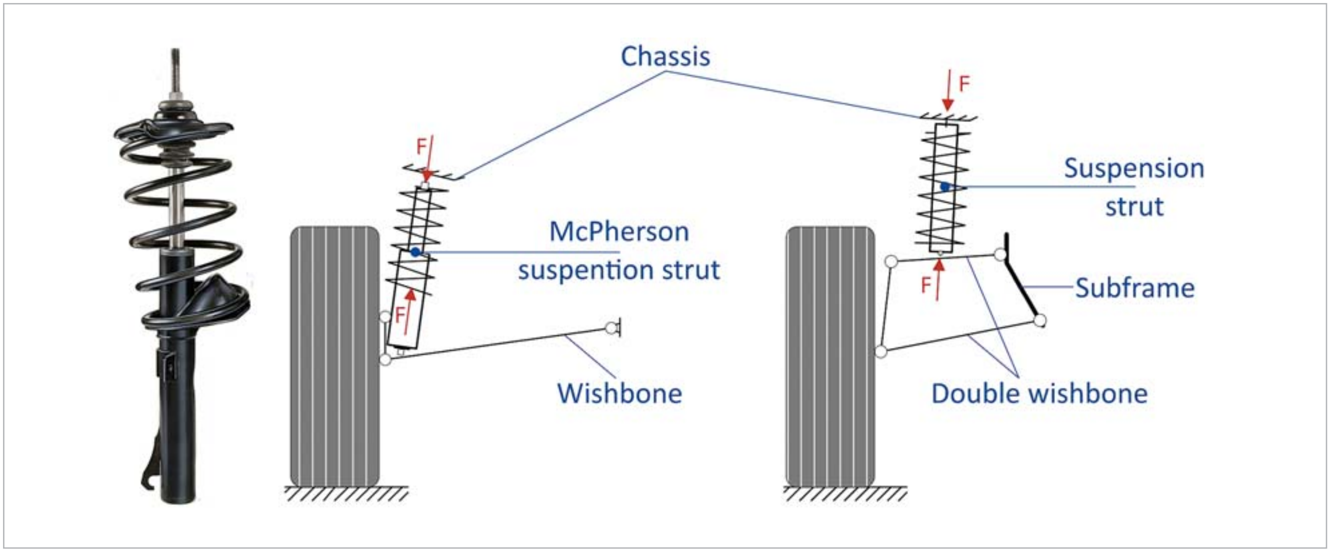

Fig. 1: Spring arrangement around the damper

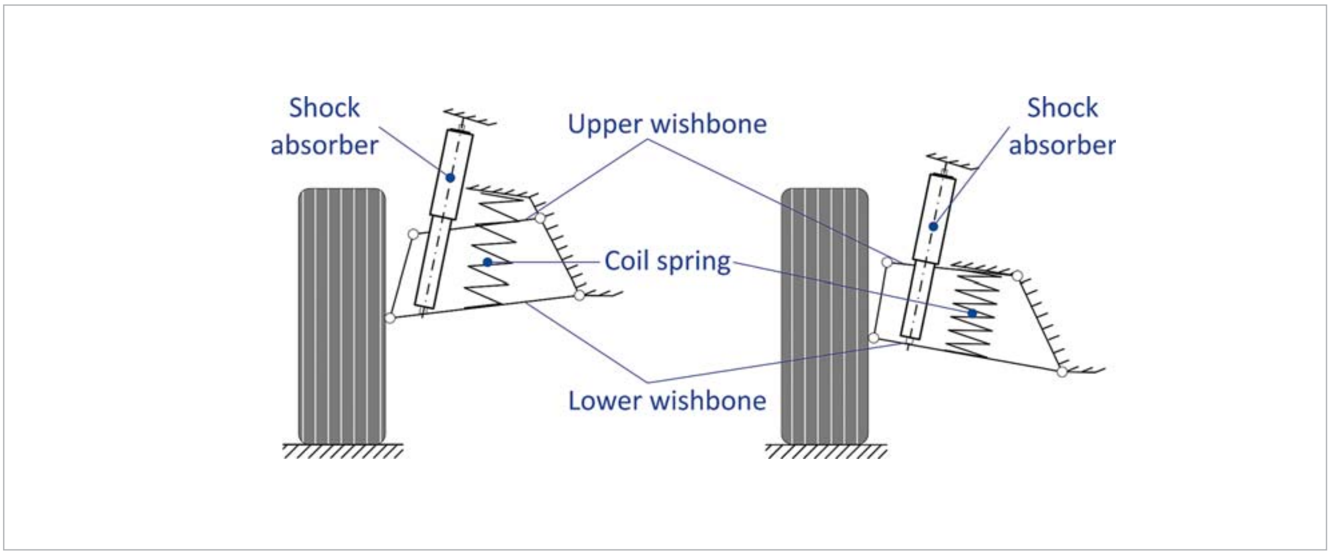

Fig 2: Spring arrangement on a wishbone: decompressed (left) and compressed (right)

an angle range up to about 270° to support a centric force transmission. The support is either constructed on flat or pitch-profiled spring seats. These are usually made of sheet metal or rubber parts that are adapted to the end coil.

The force transmission can be basically classified into two different types. The more simple technique is to guide linearly the end coil of the spring toward each other with parallel aligned struts and without any lateral offset. This variant is still interesting today because it allows a simple dimensioning of cylindrical helical compression springs (see: DIN 13906-1).

Two examples of the first type of load transmission are shown in Fig. 1. The spring is arranged around the damper forming a unit. One end is fitted to the other without lateral offset. This enables a practically free deflection of a cylindrical spring regarding bending-moment and lateral force with evenly distributed coil stress.

In many applications, however, the end coils are guided toward each other using non-parallel aligned struts with curved spatial orientation or with lateral offset. When dimensioning helical compression springs, simple methods have to be replaced by Finite Elements Analysis (FEA). Two examples of the second type of force transmission are shown in Fig. 2.

The spring is mounted on the lower wishbone and the spring end is guided along a space curve. As a result, the cylindrical spring is unevenly deformed and, in addition, moment and transverse forces are acting at both spring ends. The consequence is an uneven stress distribution in the coils and a distortion of the spring body.

Analytical dimensioning

The calculation of coil springs is based on the equations given in the standard sheet DIN EN 13906-1. The following basic formulas are taken from this standard sheet and describe the relationships between the most important characteristic values: spring rate R, spring force F, shear modulus G, wire

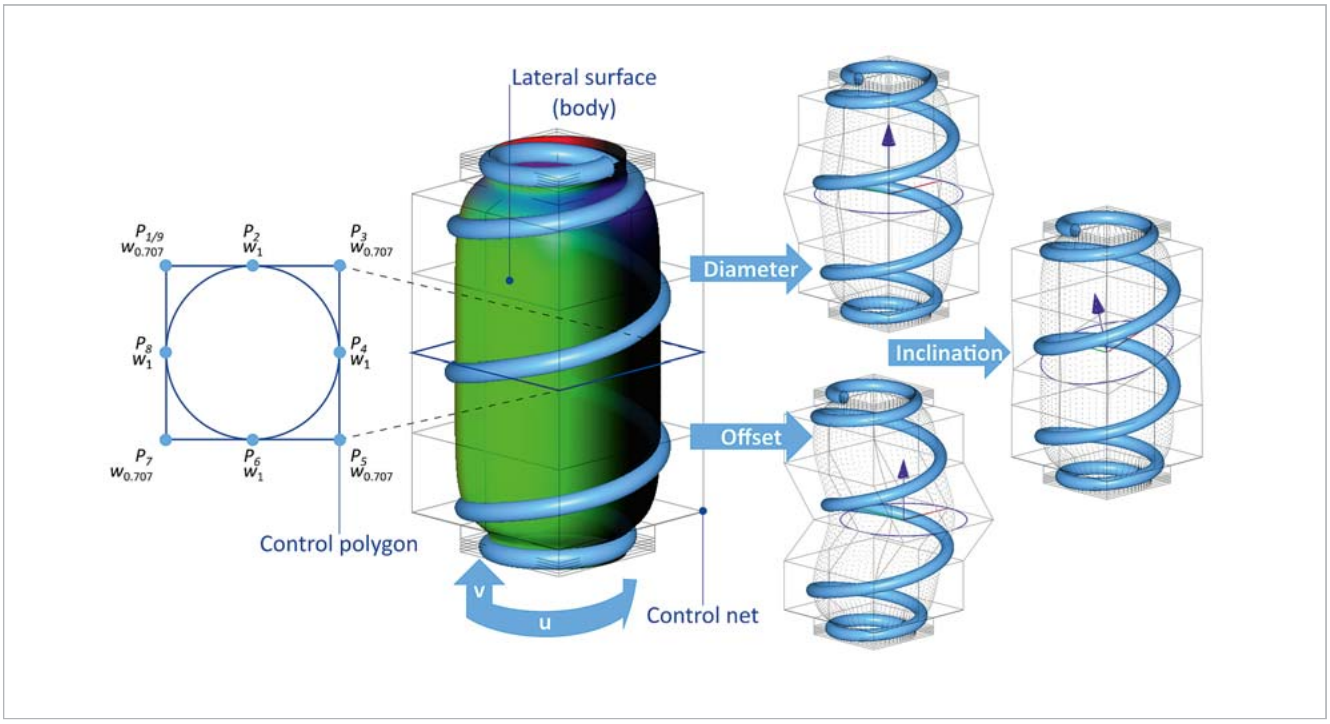

Fig. 3: Generation and variation of the lateral surface

diameter d, number of coils n, mean coil diameter D, spring deflection s and the resulting shear stress τ. These values are essential in the calculation of simple cylindrical coil springs:

Spring Force $$F = \frac{G}{8} \cdot \left(\frac{d^4 s}{D^3 n}\right) \tag{1}$$

Spring Rate $$R = \frac{G}{8} \cdot \left(\frac{d^4}{D^3 n}\right) \tag{2}$$

Shear Stress $$\tau = \frac{8}{\pi} \cdot \left(\frac{D}{d^3}\right) \cdot F \tag{3}$$

However, this approach is only suitable in a special case of force transmission for cylindrical coil springs (see paragraph type of force transmission). Therefore, this approach can only be applied for the preliminary dimensioning of a modern coil spring.

Parameterization

The use of FEA in the dimensioning and especially in the optimization of the geometry requires a parameterized model of the coil spring. In the course of time, engineers at Mubea have developed different parameterization approaches or applications for coil spring modeling. They support the product developer in the definition of the free, unloaded coil spring geometry as well as in the setting of boundary conditions. Furthermore, they enable the generation and evaluation of the FE simulation model.

One application has been especially developed for optimization and an automated design of the coil spring geometry.

GRASP Designer

The GRASP (Graphical Spring) Designer is based on the Helix definition, which is a curve that winds around the barrel of a cylinder at a constant pitch. Similarly, with this parameterization approach, the coil spring modeling is subdivided into the modeling of a lateral surface (body) and a curve ([multiply] unwinding). With regard to C- or S-shaped coil springs, the demand on the designer is to develop more or less complex bodies and spring coils while using a manageable number of parameters. One reason to choose the mathematical construct of the NURBS (Non-Uniform Rational B-Splines) as an extension of the B-splines to describe the body and the coiling was its ability to map perfectly circular curves.

The body is defined by a closed NURBS surface, which consists of control points. The control points of a NURBS surface represent the control mesh. The surface itself is defined by u in peripheral direction (the coil spring) and v in the height direction. u and v are defined in the interval [0, 1]. The degree of the NURBS surface in v is variable.

The coiling is defined by a NURBS curve. The control points of a NURBS curve represent a control polygon. The curve itself is defined by u in the interval [0, 1]. The degree of the NURBS curve is variable.

Lateral surface

The control mesh describes the lateral surface and consists of series-connected control polygons with the resulting circular curve. For a circular cross-section, each control polygon must be aligned in peripheral direction u of the shape as shown in Fig. 3 and has to represent a second degree.

In the design process or in the subsequent optimization, not the control points of the polygon or the cross section are directly varied, but the surrogate variables that represent the individual cross sections.

These surrogate values for describing a body cross-section are:
- diameter,
- displacement and
- inclination angle.

The introduction of these surrogate values is not only advantageous for a more intuitive processing of the coil spring body, but also ensures a significant reduction of the (optimization) parameters.

Coiling

A variable number of control points define the multiple coiling of the coil spring on the body or in the uv-plane of the lateral surface. The resulting control polygon is defined on the interval [0, number of coils n] in u-direction of the lateral surface and on the interval [0, 1] in v-direction.

Here, the first and last control point is fixed in (0, 0) or (n, 1), while all other points are freely displaceable in the uv-plane. The local influence of a control point on the axial spring geometry depends on the degree of the NURBS curve (see Fig. 4).

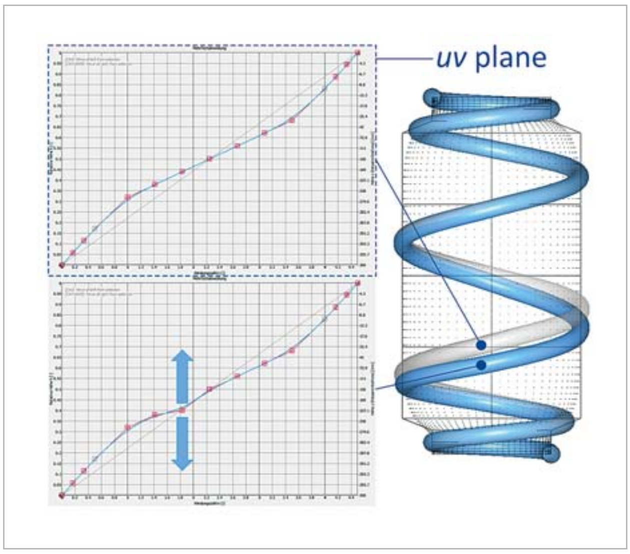

Fig. 4: Generation and variation of the coiling in the uv-plane

Simulation Model

For the numerical simulation a parameterized FE model of the coil spring is used. The simulation is done in ANSYS Mechanical APDL (ANSYS Parametric Design Language). In this case, it is a static, geometrically non-linear calculation using quadratic elements and an elastic material model.

Optimization Model

The aim of the optimization is to create a coil spring design with the required mechanical characteristics while complying with all boundary conditions and lifetime requirements. Since there are critical requirements and boundary conditions, this can be difficult to accomplish. Therefore, and to support particularly the project engineers, optimization methods are applied in the design process. An OPX file is created from GRASP on the basis of a reference design to generate the optiSLang project via the OPX interface.

In principle, an analytically generated cylindrical reference geometry is used for the automated design replacing a numerical pre-dimensioning. Due to the large number of parameters, the application of an EA optimization algorithm is required. Investigations of the existing types of mutation have shown that for the present optimization problem the constraint adaptive option has proven to be particularly stable and efficient.

Objective Function and Constraints

Coil springs are exposed to static and dynamic loads. The maximum statically permissible load is reached at maximum deflection L_{Jounce}. The assessment of the static load is based on the shear stress $\tau_{max} = \tau_{Jounce}$.

In addition to the constraint not to exceed the defined stress limit, the primary objective is to homogenize the static stress as much as possible over a considered coil area of the coil spring. Thus, an equal distribution of material stress is achieved. For this purpose, the variance of the static load is minimized.

If explicit constraints using inequalities were applied, the analyses showed a negative effect on the objective history and the quality of results, or on the stability of the automated design methodology. For this reason, all constraints included in the objective function to be minimized are defined as penalty terms. For an inequality

$$L_i \geq R_i \tag{4}$$

the penalty term P_i is

$$P_i = \frac{w_i}{2} \cdot [\mathrm{sign}(R_i - L_i) + 1] \cdot [|L_i| + 1]^{k_i} \tag{5}$$

with weighting w_i and exponent k_i

This definition includes a step function that zeroes the penalty term as soon as the originally formulated constraint inequality is fulfilled. The weighting as well as the exponent can be used to adjust the magnitude of the penalty term and, thus, its priority within the objective function. Here, the weighting mode of the penalty terms considers a violation of constraints more than an improvement of the original objective function. Therefore, it can be ensured that the optimization algorithm primarily fulfills all constraints.

For a scattering objective value C standardized to the tolerance interval, the constraints can be defined as follows:

$$\frac{C_{tol} - |C_{target} - C|}{2 \cdot |C_{tol}|} \geq 0 \tag{6}$$

For the alternative definition as a penalty term this would result in:

$$C_{penalty} = \frac{w_C}{2} \cdot \left[\mathrm{sign}\left(0 - \frac{C_{tol} - |C_{target} - C|}{2 \cdot |C_{tol}|}\right) + 1\right] \cdot \left[\left|\frac{C_{tol} - |C_{target} - C|}{2 \cdot |C_{tol}|}\right| + 1\right]^{k_C} \tag{7}$$

At this point, the following constraints are taken into account in the design of the coil spring:

- Maximum permissible limit stress
- (Nominal) supporting force Fz (± Tol.) of the coil spring at design length L_{Design} (length when installed at empty vehicle weight)
- (Nominal) spring rate R (± Tol.) in the range of $L_{Design} \pm \Delta L$
- (Nominal) piercing points $PP_{x|y,top|bottom}$ (±Tol.) at L_{Design} (Intersection of the resulting force with the upper or lower plane through spring ends)
- Minimum distance between coils
- Maximum permissible gap / clearance between coil spring ends and seat
- Design space

The space design verification is carried out on the basis of STLs. Here a separate inner and outer design space is required (see Fig. 5). Several sections are generated through the deformed coil spring and the design space STLs. Each section forms two surfaces based on the STLs. For each axial spring section, the minimum distance to the respective cut surface is determined. If the axial spring section is outside the cut surface, the minimum distance is given a negative sign, which represents a space violation corresponding to the requirement of a distance ≥ 0. The first and last half coil of the coil spring is usually excluded from the design space verification.

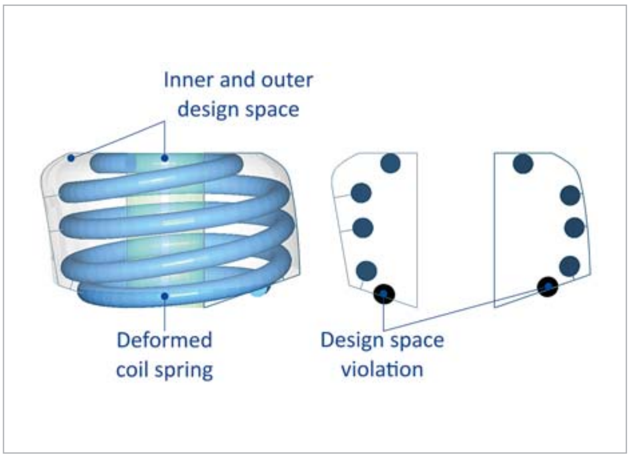

Fig. 5: Inner and outer design space limits (left) and section through design limits and coil spring (right)

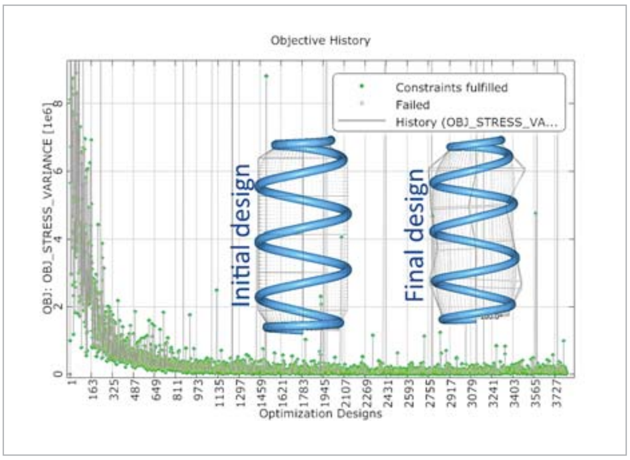

Fig. 6: Initial cylindrical coil spring design and final geometry

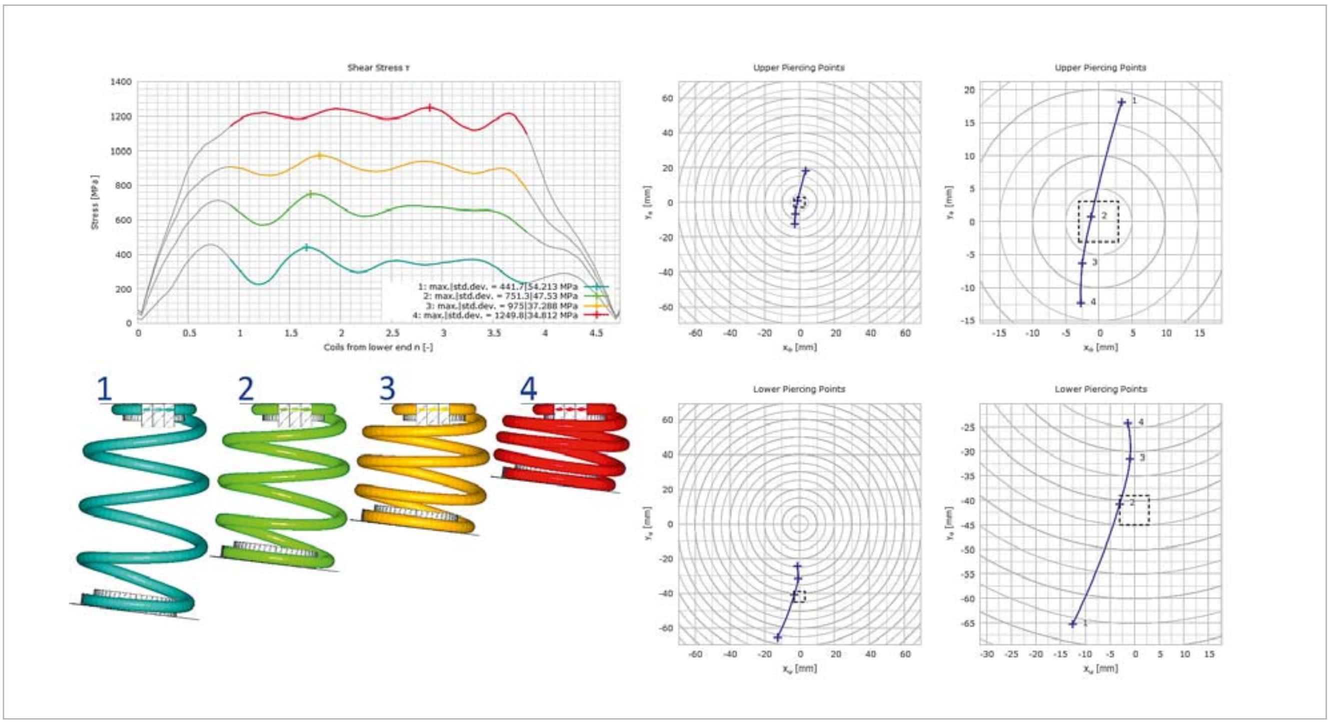

Fig. 7: Shear stress curve (left) and piercing points (right) in different compression states

Results and Conclusion

The result of an exemplary automated coil spring design with optiSLang is shown in Fig. 6 (see previous page).

A cylindrical coil spring based on an analytical pre-dimensioning was used as the initial design. The final optimized design could already be determined after running only 4000 variants. It has to be noted that the history of the objective function showed a steady and rapid improvement. This is due to the use of constraints as penalty terms in the objective function and is representative of all previous coil spring designs generated with optiSLang. The abort criterion is usually reached between 4000 and 6000 designs.

Fig. 7 (see previous page) shows selected results of the final design. On the left side, the shear stress curves are shown in different compression states for the considered coil area. The red shear stress curve corresponds to the maximum deflection and was, as required, sufficiently smoothed.

On the right side of the figure, the piercing points can be seen in evenly scaled and detailed views. There the required piercing points for compression step 2 are located within the given tolerances.

As a conclusion, it can be stated that the automated design using optiSLang is very practicable. The automated engineering procedure not only convinces with high-quality results, it also provides meaningful results, which would be difficult to achieve with manual designing. The greatest advantage of automated dimensioning is the homogenization of the stresses. Otherwise, this would be a major challenge while using manual designing procedures.

Author//
S. Schneider (Mubea Fahrwerksfedern GmbH)

ANNUAL WEIMAR OPTIMIZATION AND STOCHASTIC DAYS

Your conference for CAE-based parametric optimization, stochastic analysis and Robust Design Optimization in virtual product development.

The annual conference aims at promoting successful applications of parametric optimization and CAE-based stochastic analysis in virtual product design. The conference offers focused information and training in practical seminars and interdisciplinary lectures. Users can talk about their experiences in parametric optimization, service providers present their new developments and scientific research institutions inform about state-of-the-art RDO methodology.

Take the opportunity to obtain and exchange knowledge with recognized experts from science and industry.

You will find more information and current dates at: **www.dynardo.de/en/wosd**.

We are looking forward to welcoming you to the next Weimar Optimization and Stochastic Days.

Contact & Distributors

Worldwide

Dynardo GmbH
Steubenstraße 25
99423 Weimar
Phone: +49 (0)3643 9008-30
Fax.: +49 (0)3643 9008-39
www.dynardo.de
contact@dynardo.de

Dynardo Austria GmbH
Office Vienna
Wagenseilgasse 14
1120 Vienna
www.dynardo.at
contact@dynardo.at

Worldwide distribution of ANSYS optiSLang
ANSYS, Inc.
Canonsburg
www.ansys.com

Worldwide distribution of optiSLang
LightTrans GmbH
Jena
www.lighttrans.de

Germany
CADFEM GmbH
Grafing b. München
www.cadfem.de

Austria
CADFEM (Austria) GmbH
Vienna
www.cadfem.at

Switzerland
CADFEM (Suisse) AG
Aadorf
www.cadfem.ch

Czech Republic, Slovakia, Hungary
SVS FEM s.r.o.
Brno-Židenice
www.svsfem.cz

Sweden, Denmark, Finland, Norway
EDR & Medeso AB
Västerås
www.edrmedeso.com

United Kingdom of Great Britain and Northern Ireland
CADFEM UK CAE Ltd
Croydon, Surrey
www.cadfemukandireland.com

Ireland
CADFEM Ireland Ltd
Dublin
www.cadfemukandireland.com

Turkey
FIGES A.S.
Istanbul
www.figes.com.tr

North Africa
CADFEM Afrique du Nord s.a.r.l.
Sousse
www.cadfem-an.com

Russia
CADFEM CIS
Moscow
www.cadfem-cis.ru

India
CADFEM Engineering Services India
Hyderabad
www.cadfem.in

USA

CADFEM Americas, Inc.
Farmington Hills, MI
www.cadfem-americas.com

Ozen Engineering Inc.
Sunnyvale, CA
www.ozeninc.com

USA/Canada
SimuTech Group Inc.
Rochester, NY
www.simutechgroup.com

Japan
TECOSIM Japan Limited
Saitama
www.tecosim.co.jp

Korea
TaeSung S&E Inc.
Seoul
www.tsne.co.kr

China
PERA-CADFEM Consulting Inc.
Beijing
www.peraglobal.com

Publication details

Publisher
Dynardo GmbH
Steubenstraße 25
99423 Weimar
www.dynardo.de
contact@dynardo.de

Executive Editor & Layout
Henning Schwarz
henning.schwarz@dynardo.de

Registration
Local court Jena: HRB 111784

VAT Registration Number
DE 214626029

Publication
worldwide